Index 35726 X
ISSN 0867-888X

POLISH
ACADEMY
OF SCIENCES
INSTITUTE
OF FUNDAMENTAL
TECHNOLOGICAL
RESEARCH

NATIONAL
ENGINEERING
SCHOOL
OF METZ

ENGINEERING TRANSACTIONS

ROZPRAWY INŻYNIERSKIE - TRAITE d'INGENIERIE

QUARTERLY
VOLUME 61
ISSUE 3

WARSZAWA - METZ 2013

Faster online
http://et.ippt.pan.pl

Contents of issue 3 vol. LXI

Engineering Transactions, Vol. **LXI**, No. 3, pp. 165–236, Warszawa - Metz 2013

ENGINEERING TRANSACTIONS

Founded 1952
Appears since 1953

Aims and Scope

ENGINEERING TRANSACTIONS promotes research and practise in engineering science and provides a forum for interdisciplinary publications combining mechanics with material science, electronics (mechanotronics), medical science and biotechnologies (biomechanics), environmental science, photonics, information technologies and other engineering applications. The Journal publishes original papers covering a broad area of research activities including experimental and hybrid techniques as well as analytical and numerical approaches. Engineering Transactions is a quarterly issued journal for researchers in academic and industrial communities.

Address of the Editorial Office:
Engineering Transactions
Institute of Fundamental Technological Research
Pawińskiego 5B, PL 02-106 Warsaw, Poland

Phone: (48-22) 826 12 81 ext. 206, Fax: (48-22) 826 98 15, E-mail: engtrans@ippt.pan.pl

Abstracted/indexed in:

Applied Mechanics Reviews, Current Mathematical Publications, Elsevier, EMBASE, Engineering Village, Inspec, Mathematical Reviews, MathSci, Reaxys, Scopus, Zentralblatt für Mathematik.

http://et.ippt.pan.pl/

Address of the Editorial Office:
Engineering Transactions
Institute of Fundamental Technological Research
Pawińskiego 5B
PL 02-106 Warsaw, Poland
Phone: (48-22) 826 12 81 ext. 206, Fax: (48-22) 826 98 15
E-mail: engtrans@ippt.pan.pl

SUBSCRIPTIONS

Subscription orders for all journals edited by Institute of Fundamental Technological Research (IPPT) may be sent directly to the Publisher:
Institute of Fundamental Technological Research
e-mail: subscribe@ippt.pan.pl

Please transfer the subscription fee to our bank account:
Payee: IPPT PAN
Bank: Pekao S.A. IV O/Warszawa
Account number 05124010531111000004426875.

WARUNKI PRENUMERATY

Prenumeratę na wszystkie czasopisma wydawane przez Instytut Podstawowych Problemów Techniki PAN przyjmuje Dział Wydawnictw IPPT.

Bieżące numery Engineering Transactions można nabyć bezpośrednio w Redakcji:
ul. Pawińskiego 5B, 02-106 Warszawa
Tel.: (48-22) 826 60 22; Fax: (48-22) 826 98 15
e-mail: subscribe@ippt.pan.pl

Arkuszy wydawniczych 5.5; Arkuszy drukarskich 4.5
Papier offset. kl. III 80 g.
Skład w systemie LaTeX K. Jezierska

ENGINEERING TRANSACTIONS • *Engng. Trans.* • **61**, 3, 167–171, 2013
Polish Academy of Sciences • Institute of Fundamental Technological Research (IPPT PAN)
National Engineering School of Metz (ENIM)

Professor Piotr Perzyna
in memoriam

On June 22, 2013 Professor Piotr Perzyna passed away. With deep regret, we said goodbye to an outstanding scientist in the field of solid mechanics, the creator of the widely used theory of viscoplasticity, a specialist in problems of thermodynamics of materials, damage dynamics, and wave propagation. He was a scientific authority, inspirer, and teacher.

Piotr Perzyna was born August 1, 1931 in Niedźwiada near Łowicz. In the years 1946–1951 he attended the Secondary School named after J. Poniatowski in Łowicz, in 1951 he began his studies at the Warsaw University of Technology. The beginnings of his research and teaching activities date back to his student days. In 1953, while still a student at the Faculty of Mechanical Engineering, Technology and Construction of the Warsaw University of Technology, he was hired as an assistant in the Department of Mechanics directed by prof. Wacław Olszak. On 28 June 1956 he graduated and received his Master Degree in Engineering. Further scientific work of Professor was carried out in the newly established Institute of Fundamental Technological Research of the Polish Academy of Sciences (IPPT PAN) in Warsaw. Professor Perzyna had been involved in this research centre for more than 45 years, being successively employed in the Department of Mechanics of Continuous Media at the positions of: senior assistant since 1956, assistant professor since 1959, associate professor since 1964, professor extraordinarius since 1971, and full professor since 1978. Since January 1964 Professor Perzyna was Head of the Division of Theory of Viscoplasticity, and since February 1979 he was Head of the Division of Theory of Inelastic Materials in IPPT PAN until retirement. Since 1974 he was a member of the Scientific Council of IPPT PAN, presiding in many of its committees. For three terms he served as Head of the Section of Solid Mechanics in Committee on Mechanics of Polish Academy of Sciences. in the years 1978–1980 he was the Head of the Doctoral Study at the IPPT PAN and in the years 1980–1982 he was the Deputy Director for Research of the IPPT PAN.

In 1959, in IPPT PAN, he received a PhD degree in Technical Sciences (supervised by Prof. Wacław Olszak), and on 25 April 1963 he received a degree of Doctor of Sciences. In the years 1961–1962 he held a postdoctoral position in the team of Prof. William Prager, the Division of Applied Mathematics, Brown University, Providence, R.I., USA.

In the years 1963–1973 he taught a monographic series of lectures on the Theory of Plasticity and Thermodynamics of Inelastic Materials at the Faculty of Mathematics, University of Warsaw. In the years 1969–1970 he was an NSF Senior Fellow at the Department of Engineering Mechanics, University of Kentucky, Lexington, USA. In 1982 and 1985 he worked as an CNRS Visiting Professor at Université Poitiers in France, and in 1982 he was a Visiting Professor at Brown University, Providence, R.I., USA. In 1985 he worked as a Visiting Professor at MIT, Cambridge, Mass., USA, and as a Visiting Professor at Tokyo University, Japan. In 1988–1991 he was an DFG Visiting Professor at the Universität Hannover in Germany.

Solid mechanics was Professor's main area of research. Piotr Perzyna was a co-founder of a new discipline – the theory viscoplasticity. His work in this area became the basis for extensive research in a number of domestic and for-

eign scientific centres. Research and results achieved in the field of constitutive modelling of inelastic materials for describing localization and damage are of special interest. Professor Piotr Perzyna proposed an original way of description within the domain of the thermodynamic structure with internal parameters. The choice of a set of internal parameters is justified by both the physical basics and experimental observations. This concept has been widely used for investigation of the localization and damage phenomena in monocrystalls and polycrystalline materials by analytical methods. This period had also resulted in formulating the criteria of localization of plastic deformation. Due to this, a detailed research on the influence of different effects on the occurrence of the phenomenon of localization was done. Professor Piotr Perzyna also achieved original results in the field of instability research of plastic flow processes and in the theory of damage. The results of these studies are of particular importance for the development of numerical methods and computer simulation of plastic flow processes. The developed numerical procedures are stable and allow to study the phenomena of localization and damage. This makes them widely cited and further developed in a number of national and international research centres.

Professor Piotr Perzyna obtained very interesting results in the field of thermodynamics of inelastic materials, as well as for dynamical and wave problems. His work in the field of description of the mechanical properties of irradiated materials were of great practical and theoretical importance. It is worth noting that subjects of PhD dissertations in various foreign scientific centres (e.g. Delft University of Technology, MIT, Tokyo University, George Washington University, Grenoble University, Barcelona University of Technology) are often inspired by the results of Professor Perzyna's research.

Many chapters in the currently published scientific monographs on the theory of plasticity describe in detail Professor Piotr Perzyna's results in the theory of viscoplasticity and constitutive modelling for describing localization and damage. After retirement he did not change his way of life and remained active in the work of the Scientific Council of the Institute of Fundamental Technological Research of the Polish Academy of Sciences, came to the Institute several times a week, was actively involved as an advisor, colleague and co-author of articles with his younger colleagues or students. He was still creative and looking for new topics. For example, in the recent years, he worked with passion on the issues of existence of Hamilton's variational principle for dissipative bodies and possible consequences of the invariance of the functional of action, and a joint publication with Witold Kosiński in the Archives of Mechanics is the result of this activity.

Professor Piotr Perzyna participated in a large number of international conferences and had been invited to their scientific committees and to deliver plenary lectures. Since 1964, he participated in all International Congresses of

Theoretical and Applied Mechanics (IUTAM), presenting there papers based on his own research. At the Congress of IUTAM in Toronto in 1980, he was asked to deliver a plenary lecture. He participated in many IUTAM Symposia and EUROMECH Colloquia. He was the organizer of international conferences, responsible for the scientific level of these meetings. Because of his extensive, friendly contacts he had always been able to accumulate the most prominent scientists at these meetings, providing the highest level to the events. He organized three EUROMECH Colloquia himself in 1972, 1979, and 1986. He was also the main organizer of the XVI-th Polish Solid Mechanics Conference (Krynica 1974) and XXXIII-th Polish Solid Mechanics Conference (Zakopane, 2000). In 1978, 1980, 1988, and 1997, he organized international courses at the European Centre for Mechanics CISM in Udine, Italy. In 1981–1986 Professor Piotr Perzyna was a member of the European Committee for Mechanics (EUROMECH).

Since 1964, for 30 years he was a member of the Editorial Board of the Archive of Applied Mechanics and Engineering Transactions. From 1972 to 2002 he was a member of the Editorial Board of the Library of the Applied Mechanics, IPPT PAN. In the years 1991–1996 he was a member of the Advisory Board of the International Journal of Plasticity, Pergamon Press; from 1990 to 1996, a member of the Advisory Board of International Journal of Impact Engineering, Pergamon Press; and from 1992 to 1998, a member of the Advisory Board of the JSME International Journal of Mechanics and Material Engineering, the Japan Society of Mechanical Engineers; from 1992 to 1997 a member of the Advisory Board of the European Journal of Mechanics.

The creative achievements of Professor include six scientific monographs, two university textbooks, and about 270 original scientific works, the vast majority of which were published in reputable journals currently covered by Thomson Reuters databases. Professor's publications are widely cited, and a few of them belong to the most frequently cited Polish works in the field of technical and mathematical sciences (works from the years 1963, 1966, 1971, 1978). The theory of viscoplasticty created by Professor is widely discussed also in the most significant monographs published in prominent scientific publishing houses. Moreover, Professor is author or co-author of more than twenty books, including one of the first in the world books on plasticity in 1966. Citations of Professor's work are not limited to the publications listed in the Web of Science databases. Hundreds of doctoral and postdoctoral works referring to the issue of plasticity always discuss the fundamental results of Professor Perzyna.

Looking at the impressive number of his international research internships, professors' visits, and travels to the most prestigious conferences in the world, one can say without a doubt that he belonged to a small group of truly world scientists, for whom, even during the difficult years of our post-war history, borders did not constitute a major barrier.

Professor Piotr Perzyna had supervised 17 completed PhD theses. Nine of his co-workers gained degrees of Doctors of Sciences, and 7 became professors. Professor also inspired many other researchers, and the value of scientific discussions with him could not be underestimated. He was a researcher who excellently and effectively directed research topics of discussion participants or seminar panelists. There is a numerous group of co-workers who do not change the presented statistics, but who truly belong to the group of his students; thanks to Professor, Polish mechanics maintains and strengthens its position in the scientific world. The names of his doctoral students in the alphabetical order are: Angel Baltov, Józef Bejda, Paweł Dłużewski, Aldona Drabik, Kurt Frischmuth, Tadeusz Jeske, Witold Kosiński, Sumio Murakami, Zdzisław Nowak, Anna Pabjanek, Ryszard Pęcherski, Amalia Pielorz, Jacek Rońda, Katarzyna Szmit-Saxton, Tomasz Wierzbicki, and Włodzimierz Wojno.

Professor was a very demanding supervisor, but also an excellent and highly respected professional, colleague, and friend. His enthusiasm, high standards of ethics, and scientific honesty in an effort to solve research problems, to find an explanation of the observed phenomena, and his approach to research in general, shaped the minds of generations of co-workers. Many of his students and graduate students have become well-known scholars in Poland and beyond its borders. For example, Tomasz Wierzbicki is a professor at MIT, Angel Baltov for many years worked as the scientific director of the Bulgarian Academy of Sciences, Sumio Murakami was a professor at Nagoya University, Witold Kosiński is a professor at the Polish-Japanese Institute of Information Technology, where he worked for six years as a vice-rector for research, and Aldona Drabik is the general vice-rector there, Jacek Ronda, currently a professor at the AGH University of Science and Technology, was for many years a professor at Cape Town University, Kasia Szmit-Saxton has been for many years a professor at Loyola University in New Orleans, Paweł Dłużewski and Ryszard Pęcherski are professors at the IPPT PAN, and Kurt Frischmut is a professor at the University of Rostock.

Professor Perzyna was the winner of prestigious awards. In 1960, the M.T. Huber Prize, Division IV of the Polish Academy of Sciences; in 1968, the State team award of II degree; in 1974 and 1978, awards of the Scientific Secretary of the Polish Academy of Sciences; in 1984, individual State award of II degree; and in 1993, together with prof. Erwin Stein from Hanover, Max Plank Research Award (Max Plank Society and the Humboldt Association). In the year 2008, Professor Piotr Perzyna has been awarded the doctor Honoris Causa title by the Poznań University of Technology. Professor Piotr Perzyna was awarded the Chevalier Cross of the Polonia Restituta Order.

Witold Kosiński
Zdzisław Nowak
Ryszard Pęcherski

ENGINEERING TRANSACTIONS • *Engng. Trans.* • **61**, 3, 173–184, 2013
Polish Academy of Sciences • Institute of Fundamental Technological Research (IPPT PAN)
National Engineering School of Metz (ENIM)

Structural Behavior of Sandwich Panels with External Deep-Profiled and Internal Soft Facing

Zbigniew POZORSKI[1)], Rafał SÓL[1)], Jacek SZAJDA[1)], Jolanta BŁASZCZUK[2)]

[1)] *Poznan University of Technology, Institute of Structural Engineering*
Piotrowo 5, 60-965 Poznań, Poland
e-mail: zbigniew.pozorski@put.poznan.pl

[2)] *Czestochowa University of Technology, Institute of Mathematics*
Armii Krajowej 21, 42-200 Częstochowa, Poland

Sandwich panels made of deep-profiled steel facesheet, thick and soft PUR core and thin aluminum facesheet are considered. The structural behavior of the panel in two arrangements is analyzed by the way of real experiments. Three-point bending tests were carried out. The laboratory tests unraveled non-linear characteristics of structural behavior. The local instability of the compressed faces was observed. The real experiments were compared with the results of numerical simulations.

Key words: sandwich panels, PUR core, soft facing, experimental analysis, three-point bending, failure mechanisms.

1. Introduction

Sandwich panels which are utilized in civil engineering usually consist of thin and rigid (often deep-profiled) external facings and a thick and soft core. They are used as roof and wall cladding. Lately, sandwich panels with one face soft instead of rigid have aroused wide interest. The soft face can be made of composite paper, aluminum, elastic fibres or other materials. In spite of difficulties in production and limitations in typical applications, the producers have new product applications in view. Certainly they are also motivated by lower costs of production.

A general review of sandwich structure problems was presented by Zenkert [16] and Davies [4], while a survey of failure modes was given by Daniel *et al.* [3]. The most important aspects of structural behavior of sandwich panels are: shear deformability of the core, creep of the core, and local instability

(wrinkling) of compressed facing. Theories concerning shear deformable beams and plates are presented in [14]. The problem of creep of beams with polymer foam cores was discussed in [6].

The classical experimental approach to the wrinkling stress assessment was presented in [5]. The paper discusses the results of 3-point bending, 4-point bending laboratory tests and column compression tests. The extensive analysis of failure modes of sandwich beams was presented in [12]. This study focused on the competing collapse mechanisms for simply supported sandwich beams subjected to 3-point bending. The analysis of sandwich structure with a specific core type, namely metallic foam core, was investigated in [10]. This kind of foam can fail by several modes.

The influence of geometrical and mechanical parameters on the non-linear behavior of sandwich structures is usually studied by numerical and analytical simulations. It was presented in [9] that sandwiches are very sensitive to geometrical imperfections. The extensive parametric simulations of sandwich beams under pure bending (4-point bending) are presented in [7]. In particular, the influence of the core depth and core mechanical parameters on wrinkling failure was analyzed. Classical experimental methods often fail in the case of strongly localized effect analysis. Therefore, new methods of investigations are proposed. The application of the photoelastic method to local effects evaluation is presented in [13]. The method allows one to assess local stress concentration and the influence of the indentation process.

In sandwich structures with the soft core the shear rigidity of the panel plays a crucial role. A group of identification methods of the shear modulus of the core was described in [8]. The new method of determination of the shear rigidity was proposed in [1, 2]. The proper determination of mechanical parameters highly influences the accuracy of the prediction of sandwich structure behavior. Therefore, new and more sophisticated methods are still investigated [15].

To our surprise we found a lack of papers that concern the behavior of sandwich structures with external soft face. Static analysis of sandwich structures with one soft face is a challenge. Ordinary sandwich panel theory is not reliable in such a case because of the susceptibility of the soft facesheet. From an other point of view, treatment of the structure as a deep-profiled steel sheet with additional thermal insulation and omission of the influence of the soft face leads to improper simplifications.

2. Experimental tests

To examine sandwich panel behavior under loading, 3-point bending tests were performed. Two situations were taken into consideration. In the first case

the panel is arranged with the deep-profiled steel facesheet on the top and soft face on the bottom. The steel face is subjected to bending and compression whereas the soft face is under tension. In the second case, the panel is lying with the soft face on top. This case should result in the compression of the aluminum soft face and combination of bending and tension of deep-profiled steel facesheet. The value of the excitation force, the strains in both faces, and the displacements of the plate were measured during all the tests.

2.1. Panel geometry

Figure 1 presents the cross-section of the panel. The deep-profiled face is made of zinc-galvanized steel. The measured steel core thickness is 0.395 mm, whereas the nominal yield stress of the steel is 280 MPa. The real yield stress is even higher and equals about 350 MPa. The steel is covered by a zinc layer (zinc total thickness 0.026 mm). The thickness of the internal aluminum face is 50 μm. The PUR core thickness is equal to 40 mm in the valley and 80 mm in the rib.

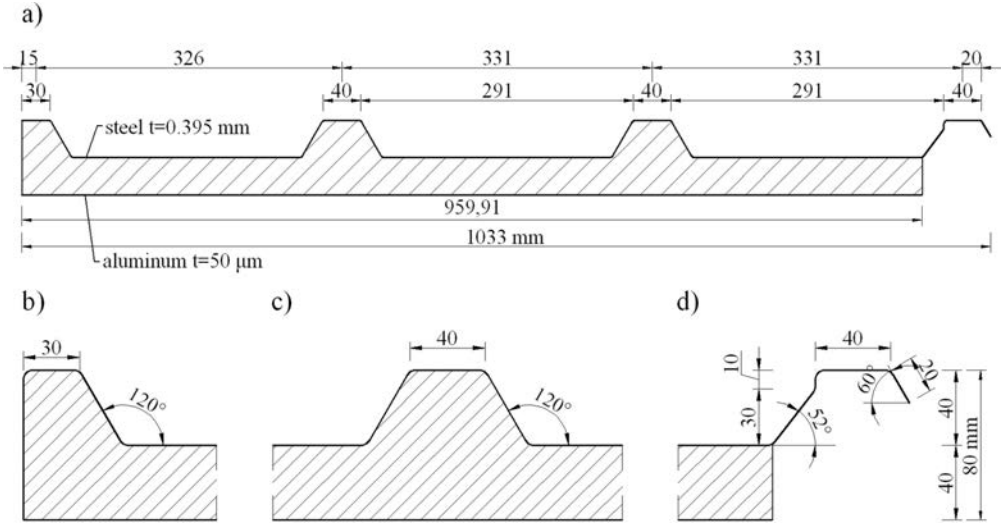

FIG. 1. The cross-section of the panel: a) overview, b) filled rib, c) rib profiling, d) free edge (longitudinal steel profiling without foam filling of the rib).

The tests were carried out on full width specimens (Fig. 1a). The total length of the panel was equal to 2.0 m. This length was chosen to provide bending failure, but the influence of the core shear is also significant. The width of the supports was 100 mm, giving the span length equal to $L = 1.90$ m. The static system is shown in Fig. 2.

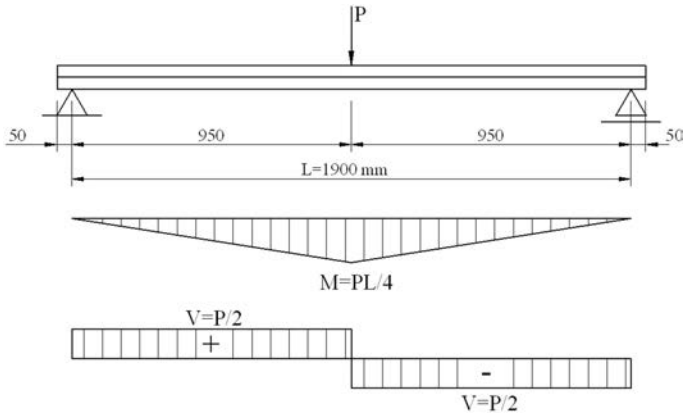

FIG. 2. The static system of the experiment (3-point bending test).

2.2. Apparatus

The test-bench consists of supporting and loading systems, force and strain gauges, and displacement transducers. The force was excited by the hydraulic jack and transferred to the panel through the loading beam. The force values were registered using the HBM C6A 50 kN load cell installed directly under the jack. Strains were measured on the both faces by HBM 10/120 LY41 linear

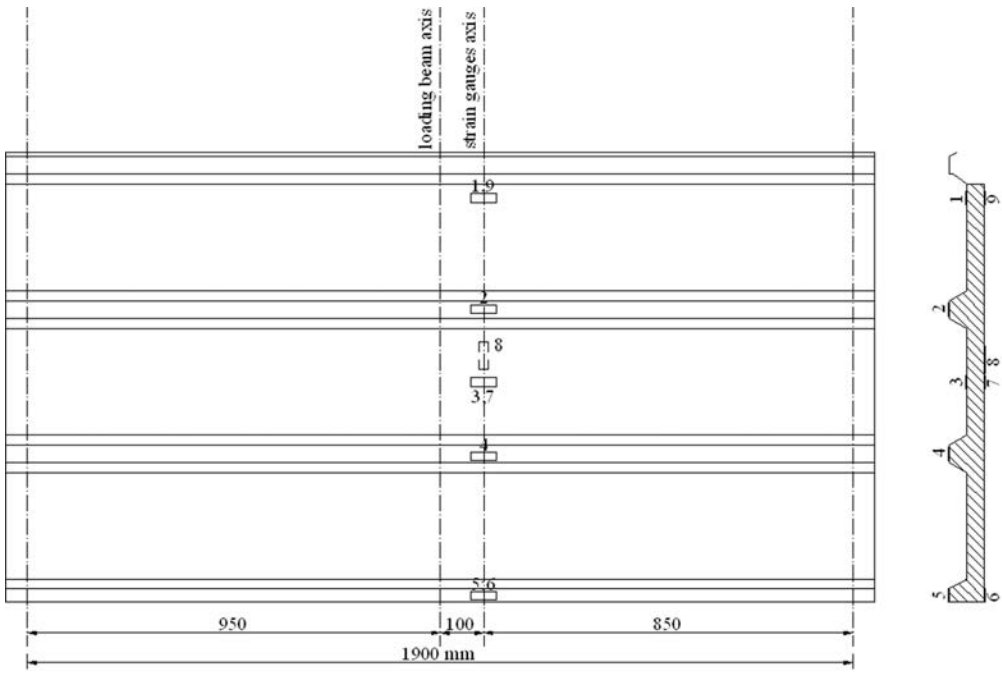

FIG. 3. The location of strain gauges.

strain gauges. All strain gauges were located at a distance of 100 mm from the loading beam axis. It limits the influence of local effects (e.g. indentation) on the strain measurements. The location of the strain gauges is specified in Fig. 3. The strain gauge numbers 1, 3 and 2, 4, 5 were placed in the valleys and on the ribs of the deep-profiled face, respectively. The strain gauge numbers 6, 7, 9 were placed on the aluminum face. Additionally, the strain gauge number 8 measured the strain of the aluminum face in the direction parallel to the loading line. The displacement transducers were mounted at both edges of the panel, in the distant 100 mm from the middle of the panel.

2.3. Situation 1 – the deep-profiled steel face on the top

In this panel arrangement the damage is related to the wrinkling of the steel ribs under compression (Fig. 4a). Tension failure of the aluminum face, and panel breakage, took place subsequently (Fig. 4b). Figure 5 shows the force-

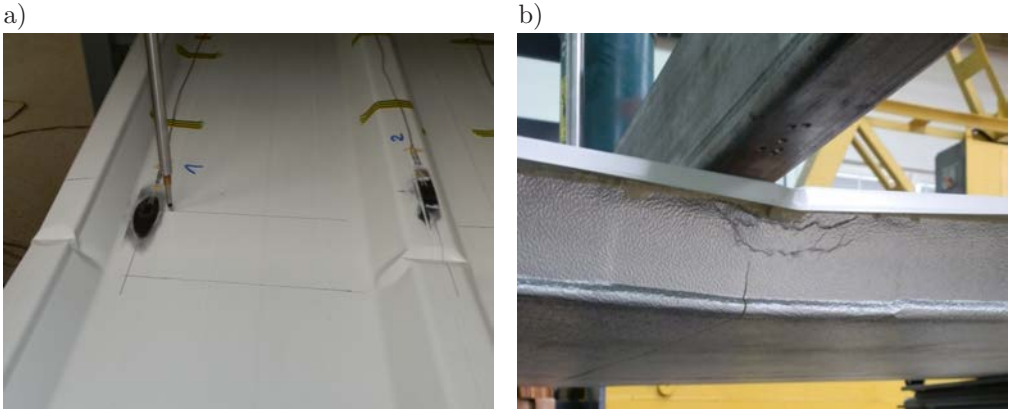

FIG. 4. The damage mechanism in situation 1: a) wrinkling of the deep-profiled steel face, b) aluminum face failure.

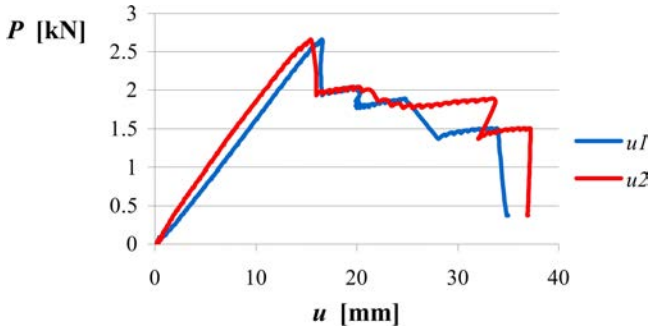

FIG. 5. The force-displacement relation in situation 1; $u1$ – the displacement measured next to the free edge of face profiling, $u2$ – the displacement measured next to the filled rib, displacement limit $L/150 = 12.67$ mm.

displacement relation in this situation. This relation is almost linear until the damage occurs. The panel displacement at the peak force $P_{\max} = 2.66$ kN is equal to 16.54 mm, which exceeds the displacement limit, $u_{\lim} = L/150 = 12.67$ mm.

To estimate the stress level in the facesheets, several assumptions were made:

- Young's modulus of the steel face is 210 GPa,
- Young's modulus of the aluminum face is 70 GPa,
- the linear part of the strain-stress relation can be expressed by Hooke's law.

The strains in the upper region of the steel face reached $\varepsilon = -0.00138$ at maximum load (Fig. 6). It corresponds to the compression stress −289.8 MPa. This means that the wrinkling stress is a little bit higher than the declared yield stress.

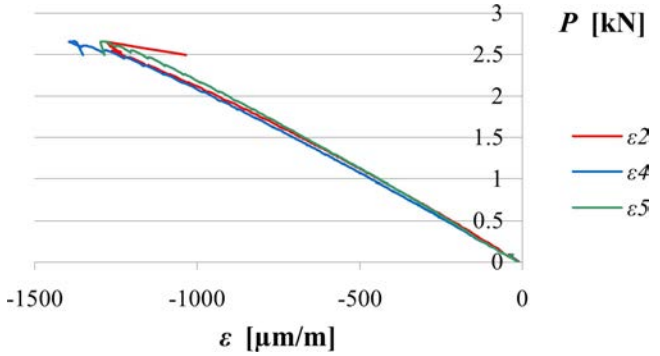

FIG. 6. Strains on the top of steel face in situation 1.

The strain in the aluminum face at a peak force $P_{\max} = 2.66$ kN was $\varepsilon = 0.00125$. Assuming Hooke's law, this gives stress 87.5 MPa. The strain measured at the moment of the tension failure was equal to $\varepsilon = 0.00306$. Figure 6 presents the estimated stress distribution within the cross-section of the panel for the peak load $P_{\max} = 2.66$ kN. Note that neither dead load nor apparatus weight were included. The additional bending moment caused by them was equal to 0.179 kNm.

The stress distribution was assessed using the measured values of strains. It needs to be emphasized that following the classical sandwich panel theory [4, 16], contrary to the classical Bernoulli beam theory, the strain distribution is not linear. The cross-section, which is initially plane, does not remain plane after deformation. The cross-section deformation is described by the superposition of the rotation of the normal element and the shear deformation of the core.

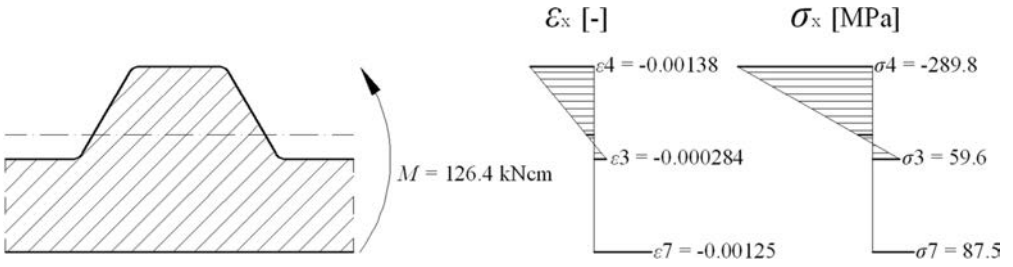

FIG. 7. The measured strains values and estimated stress distribution for $P = 2.66$ kN in the situation 1 (assuming $\sigma = E\varepsilon$).

2.4. Situation 2 – aluminum soft face on the top

In this case the failure mechanism is initiated by yielding of the tensioned part of the deep-profiled steel face. At the same time the foam core is locally deformed by the line loading. The thin aluminum paper is pressed down into the core (Fig. 8a). Since the deep-profiled facesheet is subjected to bending, the valleys of the cross-section are compressed. A high level of compression finally leads to the local instability of compressed parts of the steel facesheet (Fig. 8b).

a) b)

FIG. 8. The damage mechanism in situation 2: a) local core crushing due to line loading, b) wrinkling of the steel face in the valleys.

The force-displacement relation is evidently non-linear (Fig. 9). The displacement registered at a peak force of 3.32 kN was equal to 29.06 mm. Non-linearity occurred at the load level greater than 2.0 kN. Up to this force the displacements in both cases are comparable (situation 1: $u(P = 2.0\text{ kN}) = 11.57$ mm; situation 2: $u(P = 2.0\text{ kN}) = 12.06$ mm).

The strain in the outer part of the steel facesheet reached $\varepsilon = 0.00190$. Multiplying the strain by the Young modulus, the tensile stress 399.0 MPa is achieved,

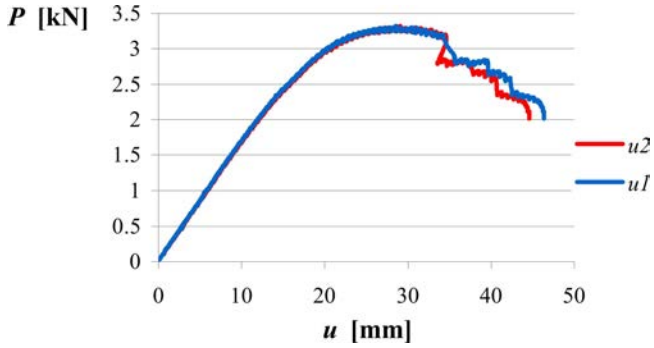

FIG. 9. The force-displacement relation in situation 2: $u1$ – the displacement measured next to the filled rib, $u2$ – the displacement measured next to the free edge of face profiling, displacement limit $L/150$=12.67 mm.

which exceeds the yield stress. More probable is a lower stress value. The strain in the compressed part of the steel face equalled $\varepsilon = -0.00080$, which corresponds to the compression stress -168.0 MPa. The measured aluminum face strain was $\varepsilon = -0.000795$, although this value is questionable. The estimated stress distribution is shown in Fig. 10.

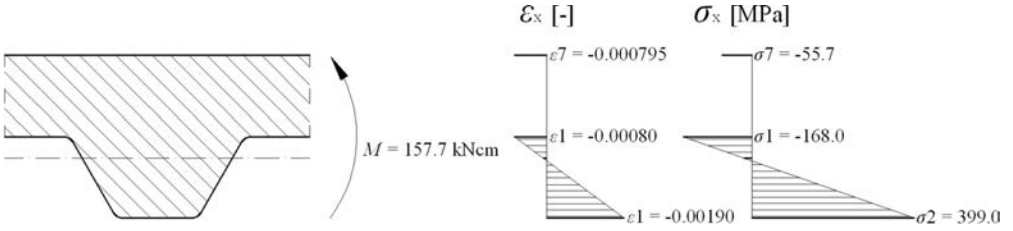

FIG. 10. The estimated stress distribution for P=3.32 kN in situation 2 (assuming $\sigma = E\varepsilon$).

The stress value in the aluminum facesheet is dubious, because there were some difficulties in attaching the strain gauges to the aluminum face. Cement that was used showed greater stiffness than the aluminum paper itself, which certainly had the influence on the experimental results.

3. Numerical simulations

3.1. Numerical model

The parameters of the numerical simulations strictly correspond to the real experiments. The simulations were prepared in the ABAQUS system environment. All materials were assumed as elastic, but also the case of elastic – ideal plastic model of steel and aluminum materials was taken into account. The core

was assumed as elastic because the extreme normal stress is in the linear range ($65.7 < 120$ kPa). Material parameters that were used are listed in Table 1. The deep-profiling facing has the thickness 0.421 mm, the resultant Young's modulus of this face is equal to $E = 202.2$ GPa and includes the influence of the zinc layer ($t_{\text{steel}} = 0.395$ mm, $E_{\text{steel}} = 210$ GPa, $t_{\text{zinc}} = 0.026$ mm, $E_{\text{zinc}} = 84$ GPa). Both faces were modeled using four nodes, doubly curved, thin or thick shell, reduced integration, and hourglass control, finite membrane strain elements S4R. The core of the panel was modeled using eight node linear brick elements C3D8R. Interactions between all parts were defined as TIE type, which makes equal displacements of nodes.

Table 1. Properties of materials used in numerical analysis.

Part	Young's modulus	Poisson's ratio	Yield stress
Steel face	202.2 GPa	0.30	350 MPa
PUR core	8.00 MPa	0.05	–
Aluminum face	70.0 GPa	0.33	95 MPa

3.2. Comparison of the results of experiments and FEM analysis

The panel displacements $u1$ and $u2$, as well as the strains at nine chosen points at different load levels, were compared. Strain values, which were taken from the numerical simulations, correspond to the localization of the strain gauges (Fig. 3). Comparisons of experimental and numerical data in both situations are presented in Table 2 and 3. The strains in the steel facesheet, which are crucial for sandwich structure load-bearing capacity, have satisfying accuracy with the experiments. The great divergence of the strains in aluminum face could be caused by several factors. First of all, accurate material properties of aluminum paper were unknown. Secondly, the cement, which was used to attach the strain gauges, had significant stiffness compared to the stiffness of the aluminum paper. Finally, the most difficult phenomenon for proper numerical estimation is the local instability of compressed, very thin, and geometrically imperfect aluminum face.

The comparisons of the strains ε as the function of the loading force P for the real experiment and numerical simulations are shown in Fig. 11 and 12. The comparisons concern situation 1 (the deep-profiled steel face on the top in the compression), the strains in the valley (point 3, Fig. 11), and on the rib (point 4, Fig. 12). The relations are almost linear, only the behavior for load greater than 2.0 kN is nonlinear. The nonlinearity is observed in the real results and in the numerical solution for the point located in the valley, in the case of the elastic-plastic definition of the materials ($\varepsilon 3$ pl).

Table 2. Comparison of the experimental and numerical results in the situation 1.

	P [kN]	$u1$ [mm]	$u2$ [mm]	Strain in the steel face ($\cdot 10^4$)					Strain in the alu ($\cdot 10^4$)			
				$\varepsilon 1$ [–]	$\varepsilon 2$ [–]	$\varepsilon 3$ [–]	$\varepsilon 4$ [–]	$\varepsilon 5$ [–]	$\varepsilon 6$ [–]	$\varepsilon 7$ [–]	$\varepsilon 8$ [–]	$\varepsilon 9$ [–]
Exp.	1.00	5.93	5.45	1.17	−4.44	1.04	−4.66	−4.43	3.09	4.46	0.321	3.26
Num.	1.00	4.98	4.73	1.37	−4.91	1.14	−4.77	−4.14	6.02	6.01	−0.112	6.22
Δ[%]*		−15.9	−13.3	16.7	10.4	9.4	2.3	−6.5	94.7	34.8	−65.2	90.8
Exp.	2.50	14.78	14.55	3.15	−12.4	2.66	−12.5	−11.8	7.44	11.4	0.238	8.84
Num.	2.50	12.46	11.81	3.42	−12.3	2.84	−11.9	−10.4	15.1	15.0	−0.279	15.5
Δ[%]*		−15.7	−18.8	8.5	−0.8	6.7	−4.7	−11.9	102.3	31.8	17.2	75.9

*Δ = (|exp data| − |num data|)/|exp data|

Table 3. Comparison of the experimental and numerical results in the situation 2.

	P [kN]	$u1$ [mm]	$u2$ [mm]	Strain in the steel face ($\cdot 10^4$)					Strain in the alu ($\cdot 10^4$)			
				$\varepsilon 1$ [–]	$\varepsilon 2$ [–]	$\varepsilon 3$ [–]	$\varepsilon 4$ [–]	$\varepsilon 5$ [–]	$\varepsilon 6$ [–]	$\varepsilon 7$ [–]	$\varepsilon 8$ [–]	$\varepsilon 9$ [–]
Exp.	1.00	5.81	5.68	−1.53	4.69	−0.96	4.57	4.47	−4.92	−4.23	−0.221	−2.96
Num.	1.00	4.32	4.67	−1.16	4.32	−1.02	4.50	4.20	−7.47	−6.54	0.024	−7.25
Δ[%]*		−25.7	−17.8	−24.1	−7.8	6.0	−1.5	−6.0	52.0	54.7	−89.1	145.1
Exp.	3.00	20.49	20.20	−6.28	17.4	−3.41	17.2	17.3	−10.1	−8.85	−2.41	−3.62
Num.	3.00	12.95	14.02	−3.48	13.0	−3.06	13.5	12.6	−22.4	−19.6	0.072	−21.8
Δ[%]*		−36.8	−30.6	−44.6	−25.5	−10.2	−21.6	−27.0	122.4	121.7	−97.0	500.4

*Δ = (|exp data| − |num data|)/|exp data|

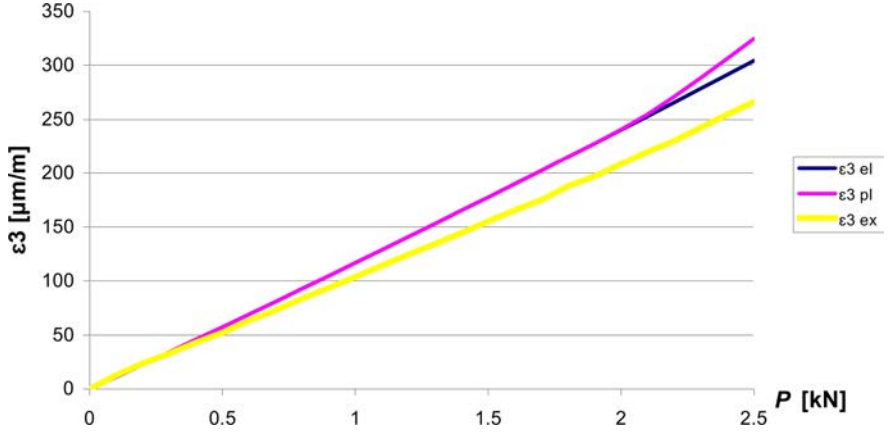

FIG. 11. The relation $\varepsilon(P)$ for the point 3 located in the valley: $\varepsilon 3$ ex – experimental results, $\varepsilon 3$ el – numerical results, elastic materials, $\varepsilon 3$ pl – numerical results, elastic-plastic materials.

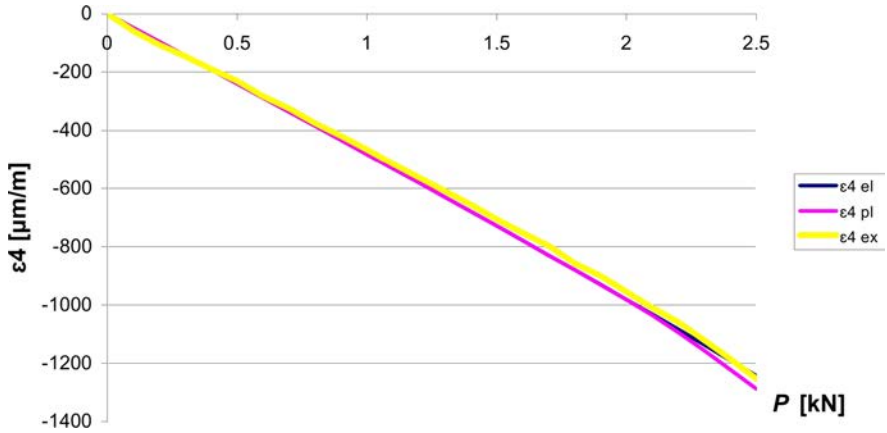

FIG. 12. The relation $\varepsilon(P)$ for the point 4 located on the rib: $\varepsilon 4$ ex – experimental results, $\varepsilon 4$ el – numerical results, elastic materials, $\varepsilon 4$ pl – numerical results, elastic-plastic materials.

4. CONCLUSIONS

The presented results show that behavior of sandwich panels with one rigid and one soft face is very interesting. The failure mechanism depends on the arrangement of the panel. In the case of a compressed deep-profiled steel face the damage is related to the wrinkling of the steel ribs. In the case of the aluminum soft face on the top, the failure is initiated by yielding of the steel face and the local foam core crushing. Finally, bending of the structure leads to the local instability of the compressed part (valley) of the steel facesheet.

From the practical point of view, better results were achieved in the case of the deep-profiled face located on the bottom. The limit load is higher in this case by about 20% and the range of nonlinear behavior is broader. It is the opinion of the authors, that such a system is safer. The enhancement of the carrying capacity is possible by increasing of the steel face rigidity (thicker face, more ribs, deeper profiling) or application of the second stiff facesheet instead of soft aluminum paper. Unfortunately, all these operations cause an increase of the costs of the panel production.

Contrary to all expectations, the bending capacity of the analyzed structure with the soft face is much higher than the capacity of the pure steel profile. According to FEM analysis presented in [11], the bending capacity of sandwich structure with soft face is at least 25% higher than the capacity of steel profile itself, not to mention about greater stiffness and higher thermal insulation. Conducted experiments indicate that soft core and soft aluminum face cooperate with the deep-profiled steel face. It encourages applying such panels as the roof covering with an additional waterproof layer placed on the top of the sandwich.

References

1. Chuda-Kowalska M. *et al.*, *Experimental determination of shear rigidity of sandwich panels with soft core*, Proc. of 10th International Conference Modern Buildings Materials, Structures and Techniques, Vol. I, P. Vainiunas and E.K. Zavadskas [Eds.], Vilnius, Lithuania, VGTU, 56–63, 2010.
2. Chuda-Kowalska M., Garstecki A., *Determination of materials constants for sandwich panels with PUR core* [in Polish: *Wyznaczanie stałych materiałowych dla płyt warstwowych z rdzeniem PUR*], Przegląd budowlany, **3**, 67–72, 2012.
3. Daniel I.M., Gdoutos E.E., Wang K.-A., Abot J.L., *Failure modes of composite sandwich beams*, Int. J. Damage Mechanics, **11**, 309–334, 2002.
4. Davies J.M., *Light Weight Sandwich Construction*, Blackwell Science, 2001.
5. Gdoutos E.E., Daniel I.M., Wang K.-A., *Compression facing wrinkling of composite sandwich structures*, Mechanics of materials, **35**, 511–522, 2003.
6. Huang J.S. *et al.*, *Creep of sandwich beams with polymer foam cores*, Journal of Materials in Civil Engineering, **2**, 3, 171–182, 1990.
7. Jasion P., Magnucki K., *Face wrinkling of sandwich beams under pure bending*, Journal of Theoretical and Applied Mechanics, **50**, 4, 933–941, 2012.
8. Juntikka R., Hallstorm S., *Shear characterization of sandwich core materials using four-point bending*, Journal of Sandwich Structures and Materials, **9**, 1, 67–94, 2007.
9. Léotoing L., Drapier S., Vautrin A., *Nonlinear interaction of geometrical and material properties in sandwich beam instabilities*, Int. J. Solid and Structures, **39**, 3717–3739, 2002.
10. McCormack T., Miller R., Kesler O., Gibson L., *Failure of sandwich beams with metallic foam cores*, Int. J. of Solids and Structures, **38**, 4901–4920, 2001.
11. Sól R., Szajda J., *Stress and strain analysis in sandwich panels with one metal facing subjected to bending* [in Polish: *Analiza stanu naprężenia i odkształcenia w zginanych płytach warstwowych z jednostronną okładziną stalową*], Poznan University of Technology, 2012.
12. Steeves C.A., Fleck N.A., *Collapse mechanisms of sandwich beams with composite faces and a foam core, loaded in three-point bending. Part II: experimental investigation and numerical modelling*, Int. J. of Mechanical Sciences, **46**, 585–608, 2004.
13. Thomsen O.T., Frostig Y., *Localized bending effects in sandwich beams: photoelastic investigations versus high-order sandwich theory results*, Composite Structures, **37**, 97–108, 1997.
14. Wang C.M., Reddy J.N., Lee K.H., *Shear deformable beams and plates*, Elsevier, 2000.
15. Zang S., Dulieu-Barton J.M., Fruehmann R.K., *A methodology for obtaining material properties of polymeric foam at elevated temperatures*, Experimental Mechanics, **52**, 1, 3–15, 2012.
16. Zenkert D., *An Introduction to sandwich construction*, Chameleon Press Ltd., London, 1995.

Received February 13, 2013; revised version March 21, 2013.

ENGINEERING TRANSACTIONS • *Engng. Trans.* • **61**, 3, 185–195, 2013
Polish Academy of Sciences • Institute of Fundamental Technological Research (IPPT PAN)
National Engineering School of Metz (ENIM)

Numerical Simulation of Impact Behaviour of Structures with Internal Pressurization for Crash-Adaptive Concept

Miguel NOVERSA, Nuno PEIXINHO

Universidade do Minho, Departamento de Engenharia Mecânica, Campus de Azurém
4800-058 Guimarães, Portugal
e-mail: peixinho@dem.uminho.pt

This study presents an alternative approach for the absorption of impact energy that uses the internal pressurization of structures in the framework of a crash-adaptive response. Numerical simulations were conducted on the axial impact of thin-walled tubular structures with circular cross-section that serves as an approximation to a front crash box of a motor vehicle. The main objective of this work consists in studying the effect of internal pressurization of tubular structures in a crashworthiness application, as well as the possibility to obtain a reduction in wall thickness thus improving weight efficiency. A numerical study is presented for an internal pressure of 20 bar and tubular structures of circular section and 1.14 mm thickness. Numerical simulations were performed by making use of the LS-DYNA explicit dynamics software, while considering for the material a stainless steel alloy that is a material with interest for crashworthiness applications and manufacturing requisites due to its balance between strength, ductility, and energy absorption. The results obtained allow the conclusion, that with respect to internal pressurization it is feasible to reduce the wall thickness and have an impact resistance identical to the original while improving overall efficiency.

Key words: numerical simulation, LS-DYNA, energy absorption, crashworthiness.

1. Introduction

Currently there is an increase in vehicle speeds, as is frequently reflected in an increase of accidents. In order to reduce the impact on occupants as well as the financial cost, manufacturers have been investing in the development of vehicle structures while considering increasing requirements of crashworthiness. With technological progress, new solutions for systems that absorb impact energy have been presented.

Moreover, reducing the weight of a vehicle structure has become a major concern in the automotive industry. In fact, a weight reduction of car structures will cause a reduction in fuel consumption and therefore a decrease of pollutant emissions. Theoretical studies show that a 100 kg reduction in the weight of a car

could save 0.2 to 0.5 litres of fuel per 100 km, assuming a normal propulsion mechanism and depending on the usage scenario [1].

However, to date, thickness reduction of a given component must involve the use of materials of higher strength and frequently higher manufacturing cost. In order to counteract this, the need arises for the use of alternatives for structural design, drawing up new strategies and devices for energy absorption. These devices can be reversible or irreversible [2]. Reversible devices are characterized by absorbing and returning energy at impact, not suffering any permanent damage to its structure. The irreversible device absorbs impact energy becoming deformed permanently, for example, as a thin-walled tubular structure with circular cross-section.

Up to now, crash adaptive safety applications are introduced in passenger cars mainly for interior, restraint, and seat applications. The optimization and pre-activation of restraint systems in advance of a physical impact lead to various benefits, such as lower speed deployment of the driver and passenger airbags, as well as improved belt action due to pre-strengthening. Having sensor information available, one has the ability to prepare vehicle structures in advance of an impact and obtain a controlled crash response resulting on a tailored crash pulse.

Having crash performance, weight restrictions, and packaging aspects in mind, one technical solution that appears as an attractive approach to create overall benefits is the use of pressurized structures. Two approaches can be used [3, 4]:

- In the first approach the initial structural shape of the crashworthy components remains unchanged during pressurization, therefore, pressure has to be adjusted carefully.
- In the second approach the implementation is performed in a way that the structure expands from a small cross-section to a larger one when being pressurized. This effect can provide great benefits, such as packaging benefits or extending the crash length.

In this work, emphasis is given to a mechanism for energy absorption of irreversible type and corresponding to the first approach (pressurization without plastic deformation – Fig. 1). The study is performed according to numerical simulation of the impact behavior of a thin-walled tubular structure, consisting in this approach to a front crash box of an automobile. This structure has circular cross section and internal pressurization will be implemented in order to allow a reduction in wall thickness (Fig. 1). Consideration will be given to the impact speed of the EuroNCAP frontal crash test (64 km/h) and a common Drop Test (36 km/h). As regards to the impact mass, this is set numerically as a moving rigid wall of 76 kg. The material used to simulate the component will be

a austenitic stainless steel (Nirosta H400) due to its excellent mechanical properties that give it a possible use in structures designed for crashworthiness [5]. The simulations are performed using LS-DYNA, a well known software used to solve various engineering problems in areas such as, crashworthiness, occupant protection in vehicles, metal deformation, drop test, impact at high speeds, and biomedical and seismic analysis, among others [6].

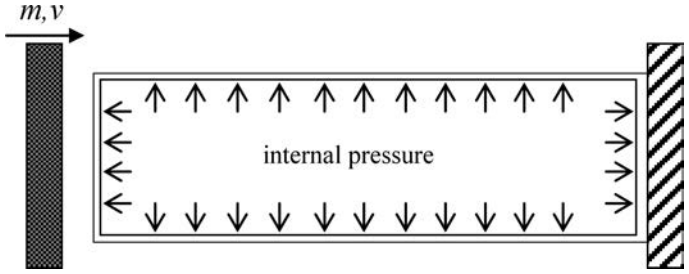

FIG. 1. Concept of pressurized cylindrical tubular structure.

Initially, a first study is performed as a numerical simulation of a tubular structure with circular cross-section of 1.14 mm thickness, which fits the hypothesis of using the same internal pressurization. The purpose is to study the influence of pressure in the interior of a structure for crashworthiness applications.

In the following step is analyzed the possibility to obtain a reduction in wall thickness of the tubular structure, using an internal pressure of 20 bar in order to attempt to compensate for the reduction in material thickness. This pressure value is usually obtained in airbag applications. Comparisons are performed between different thicknesses and internal pressure combinations. A measure of the structural efficiency for crashworthiness purposes (η) is used in the analysis through Eq. (1.1) [2], where P_m is the mean crushing load, A is the section area, and σ_y is the yield stress of the material. The mean crushing load is defined by Eq. (1.2) with δ_f as the total displacement and E_a the absorbed energy,

$$\eta = \frac{P_m}{A\sigma_y}, \tag{1.1}$$

$$P_m = \frac{E_a}{\delta_f}. \tag{1.2}$$

2. Numerical model

The crushing behaviour of thin-walled tubes was investigated with an explicit elasto-plastic finite element code: LS-DYNA. This code uses a Lagrangian formulation with a finite element mesh fixed in the material that distorts with it.

The equations of motion are integrated in time explicitly using central differences. The method requires very small time steps for a stable solution, thus it is particularly suited for impact and crash simulations though less appropriate for equilibrium structural analyses.

The finite element model is presented in Fig. 2. In the model considered, triggers are present to initiate the deformation on a prescribed position, and therefore obtain a more controlled crushing process and reduce the maximum force. The tubular structure is assumed to deform under the following constraint conditions: one end is fixed, with all degrees of freedom constrained in the distal surface nodes, and the other end is impacted by a rigid wall having a mass m and travelling with initial impact velocity v. The model was constructed using 4 node quadrilateral Belytschko-Tsay shell elements with 5 through-thickness Gauss points. An average element size of 5 mm was used. Geometric imperfections were introduced in the form of nodes displaced 0.5 mm out of plane in sympathy with the expected mode of collapse in order to trigger the analysis. Material model number 24 ("Mat_Linear_Isotropic_Plasticity") from the LS-DYNA model library was used. The true stress-strain curves were introduced in LS-DYNA, the material curve used is presented in Fig. 3 [5]. The strain-rate dependence was included through the Cowper-Symonds coefficients D and p [5]. A summary of the material properties used is presented in Table 1. The contact between the mass (rigid wall) and the specimen was modelled using a "Contact_automatic_nodes_to_surface" interface with a friction coefficient of 1.0 to prevent any sliding between specimen and wall. To account for the contact between the lobes during deformation, a "Contact_automatic_single_surface" algorithm with friction coefficient equal to 0.1 was specified.

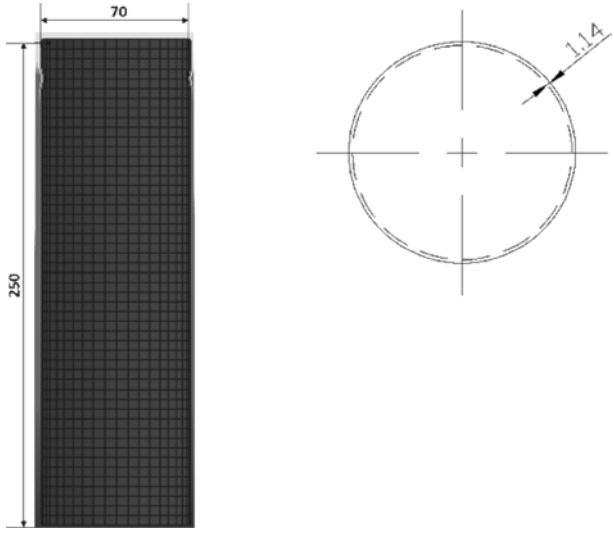

FIG. 2. Numerical model LS-DYNA and tubular section.

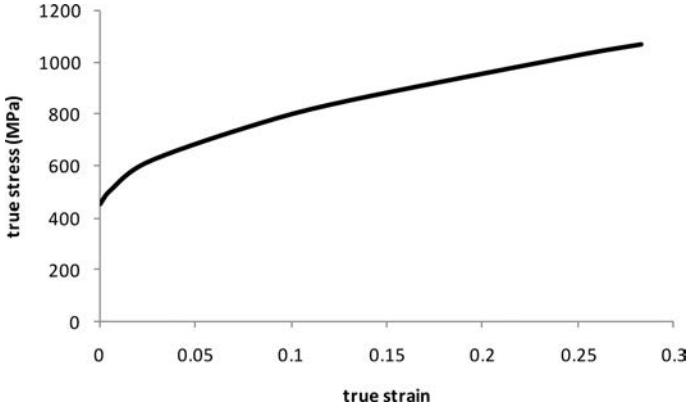

FIG. 3. Characteristic curve of austenitic stainless steel H400 [5].

Table 1. Material parameters used in numerical simulation [5].

	E [MPa]	ρ [Ton/mm^3]	σ_y [MPa]	σ_r [MPa]	Cowper-Symonds Constants	
					D [s^{-1}]	p
Stainless Steel H400	210e+5	7.38e-9	453	799	1150	7.75

The internal pressure was applied using the keyword *load* and option SHELL_SET to apply pressure to the internal shell surface within the prescribed duration time of the test, corresponding to a constant pressure application.

3. Results and discussion

3.1. Influence of internal pressure

Table 2 shows the tests initially carried out on tubular structures with a thickness of 1.14 mm. At this stage the target is to study the influence of internal pressurization at 20 bar. It should be noted, that with reference to additional internal pressure, this means that the internal pressure at 0.0 MPa is atmospheric (0.1 MPa which is approximately 1 bar). The nomenclature used is the following: **Test Name = Thickness_Impact Speed_Aditional Inside Pressure.**

Table 2. Tests carried out initially on 1.14 mm thickness structure.

Test name	Thickness [mm]	Impact velocity [mm/s]	Pressure [MPa]	Impact mass [kg]
1.14_10014_0.0	1.14	10014	0.1	76
1.14_10014_2.0	1.14	10014	2.0	76
1.14_17777_0.0	1.14	17777	0.1	76
1.14_17777_2.0	1.14	17777	2.0	76

Results for this study can be observed in Table 3, where δ_f is the total displacement, E_a is the energy absorbed, P_m is the mean crushing force, and η is the efficiency of the structure for crashworthiness purposes, as defined by equation (1.1) [2]. The percentage improvement of P_m is also given. Considering the tests conducted the same impact velocity, we can observe that the total displacement was reduced with the introduction of internal pressure while the mean load and the efficiency of the structure also increased. Figure 4 illustrates the load vs

Table 3. Results for initial tests conducted on structure with 1.14 mm of thickness.

Test name	δ_f [mm]	E_a [kJ]	P_m [kN]	P_m improv. [%]	η [%]
1.14_10014_0.0	54	3.9	72.4	–	64.8
1.14_10014_2.0	46	3.7	82.0	13.3	73.5
1.14_17777_0.0	159	12.1	76.0	–	68.1
1.14_17777_2.0	131	11.9	90.7	19.33	81.3

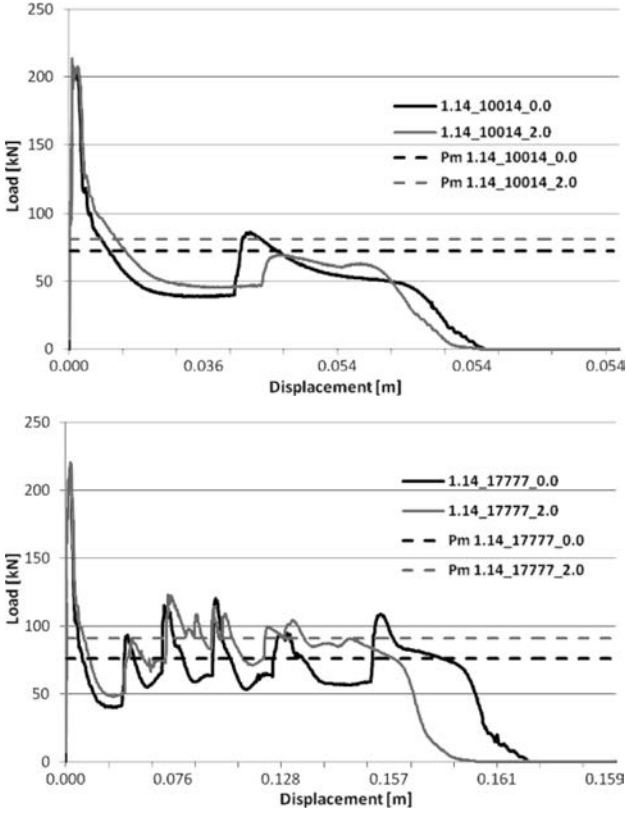

FIG. 4. Load vs. Displacement curve as tests results for 1.14 mm wall thickness structure.

displacement curves for these initial tests as well as the associated mean crushing forces. Figure 5 presents deformed shapes observed during the simulation test, where it is noted that the collapse mode does not change significantly with the introduction of internal pressure.

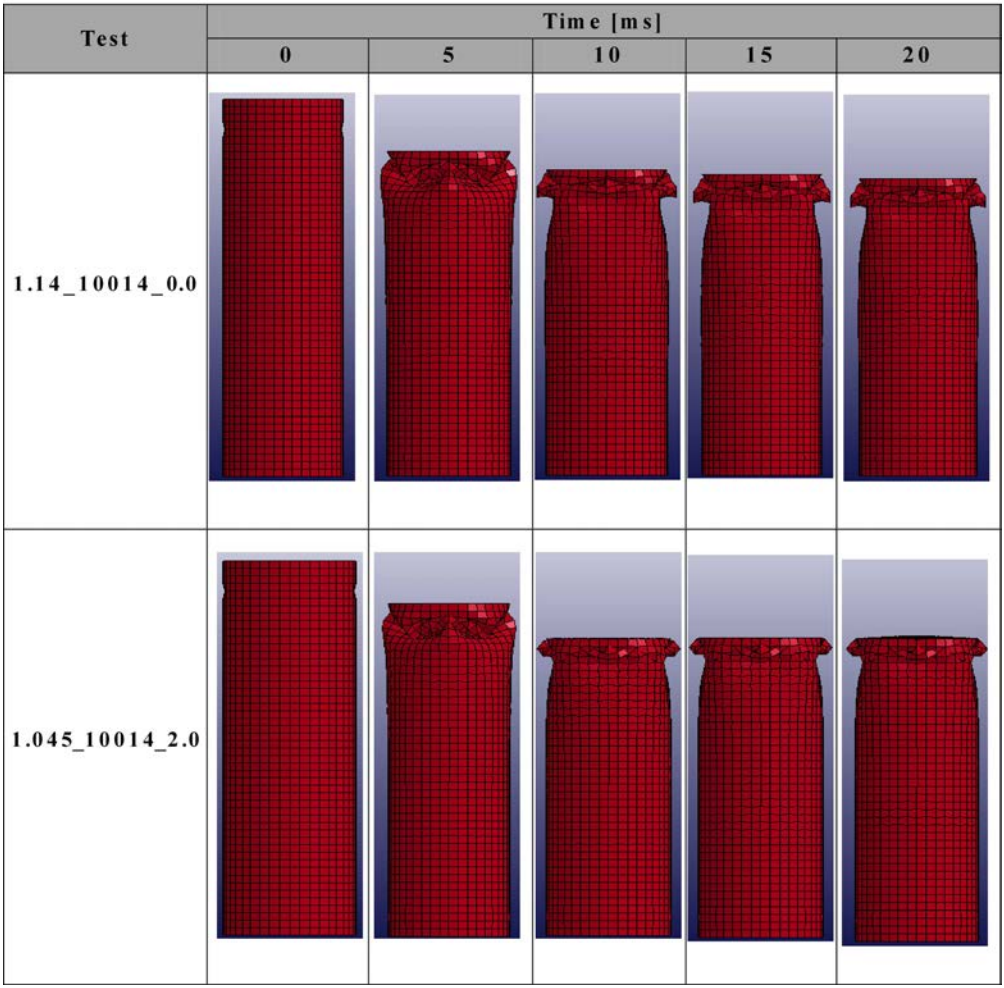

FIG. 5. Deformed shapes during simulation.

3.2. Thickness reduction

In this second stage, a study was conducted as regards the possibility of reducing the wall thickness of the structure. It was desired to maintain the same impact performance by introducing an internal pressure of 20 bar in the structure so as to offset the reduction in material thickness. Several tests were

conducted at the higher speed of 17777 mm/s, which gradually reduced the wall thickness to internal pressurisation of 20 bar. The objective was to compare the displacement of the structure with a thickness of 1.14 mm without the aditional internal pressure and the displacement of the new thinner structure with internal pressure of 20 bar. The results are presented in Table 4 and Fig. 6.

Table 4. Strategy for determination of new thickness.

Velocity [mm/s]	17777					
Internal pressure [bar]	1 bar	20 bar				
Wall Thickness [mm]	1.14	1.08	1.06	1.05	1.045	1.04
δf [m]	0.159	0.152	0.155	0.158	0.159	0.160

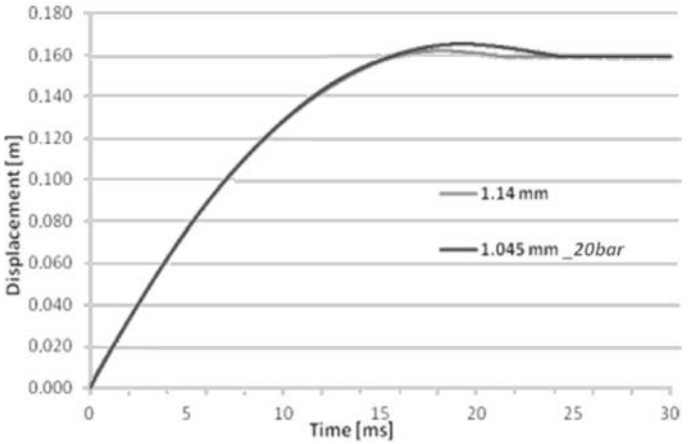

FIG. 6. Displacement vs. time curve used to determine new wall thickness.

The same total displacement was obtained for the structure with a thickness of 1.14 mm without internal pressure and the structure with a thickness of 1.045 mm with 20 bar of internal pressure. Therefore a new circular tubular structure with wall thickness of 1.045 mm was considered for further analysis. In Table 5 the results are presented for this new structure, including the per-

Table 5. Results for tests conducted on structure with 1.045 mm of thickness.

Test	δ_f [mm]	E_a [kJ]	P_m [kN]	P_m improv. [%]	η [%]
1.045_10014_0.0	67	3.9	58.6	–	57.1
1.045_10014_2.0	55	3.8	68.8	17.4	67.1
1.045_17777_0.0	189	12.1	64.0	–	62.4
1.045_17777_2.0	159	11.9	74.6	16.6	72.8

centage improvement for the new thickness. Figure 7 illustrates the variation of the mean load and load vs displacement curves for the tests conducted on the tubular structure with a thickness of 1.045 mm (for two velocities, with and without additional inside pressure).

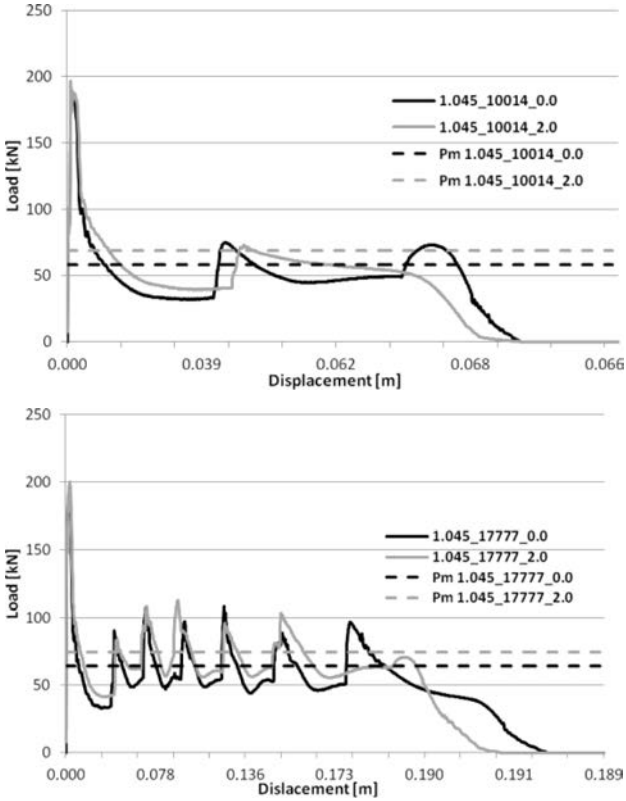

FIG. 7. Load vs. displacement curves as tests results for 1.045 mm wall thickness structure.

3.3. Comparison of results

Considering the results obtained in the simulation for the two structures, it is important to obtain a comparison between them, especially the first for non-pressurized tests (original thickness) and additionally the second with internal pressure of 20 bar (structure with 10.45 mm thickness). In Table 6 the comparitive results are compared. Figure 8 presents load vs displacement curves and the associated mean crushing forces.

For the same impact speed, identical results were obtained for both structures (1.14 mm vs pressurized 1.045 mm). The total displacement, energy absorbed,

Table 6. Comparison of results for both structures.

Test	δ_f [m]	E_a [kJ]	P_m [kN]	η [%]
1.14_10014_0.0	0.0539	3.9	72.4	64.8
1.045_10014_2.0	0.0548	3.8	68.8	67.1
1.14_17777_0.0	0.1592	12.1	76.1	68.1
1.045_17777_2.0	0.1593	11.9	74.6	72.8

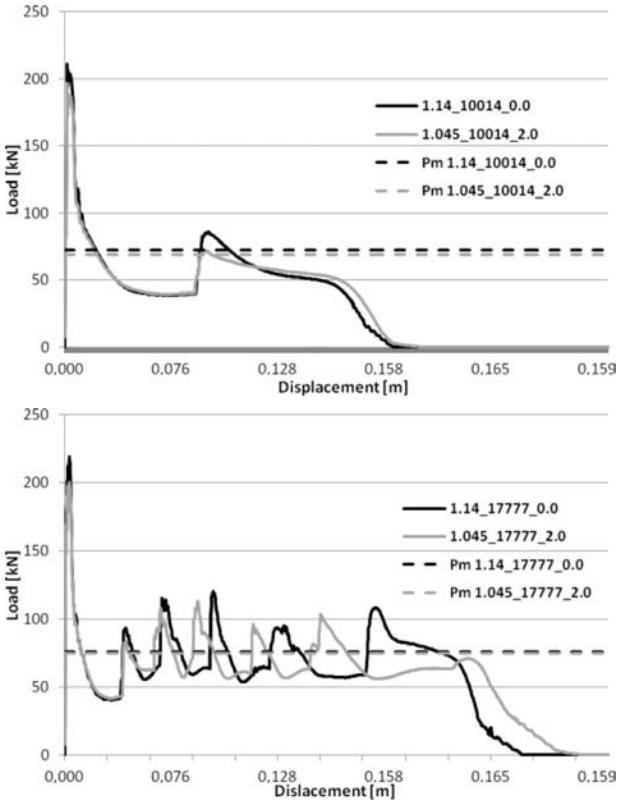

FIG. 8. Results Comparison with load vs. displacement curves for both impact velocities.

and mean load were similar considering the intended purpose, while crash efficiency increased.

4. Conclusions

A numerical study was performed on the simulation of a tubular structure with circular section and thickness of 1.14 mm, which fits in the type of structure for crashworthiness application. The purpose was to study the influence of pres-

sure inside the structure for crashworthiness applications. Based on the available results it can be concluded that it is possible to increase the impact resistance of the structure with the introduction of pressure in its interior which would benefit from its use in crashworthiness applications. The deformation decreased with increased internal pressure and the average load increased. Therefore the structure efficiency increased with the introduction of internal pressure.

Subsequently the possibility to obtain a reduction in wall thickness of the tubular structure was studied using an internal pressure of 20 bar in order to attempt to compensate this reduction. Comparisons were made between the original structure with no pressure in its interior and the thinnest structure with 20 bar of internal pressure. The results obtained allow us to conclude that it is feasible to reduce the wall thickness and have an impact resistance equivalent to the original while improving overall efficiency. For the same impact speeds, the total displacement experienced by the structure is identical, the impact energy absorbed was practically the same and, even considering a decrease of mean crushing force, there is an increase in the efficiency of the structure for impact energy absorption.

The results obtained with numerical simulations show good indications for the validity of an adaptive crashworthiness concept wherein tube pressurization could act as an enhancement of energy absorption. Such final validation is dependent on experimental results, while the implementation of a pressurization scheme and deployement parameters could be better described with a coupled fluid-structure numerical model.

References

1. Cheah L., Evans C., Bandivadekar A., Heywood J., *Factor of Two: Halving the Fuel Consumption of New U.S. Automobiles by 2035*, Project Report Publication No. LFEE 2007-04 RP, Laboratory for Energy and Environment, MIT, 2007.
2. Jones N., *Structural Impact*, Cambridge University Press, 1997.
3. Nohr M., Blume K., *Crash adaptive vehicle structures and components*, DAIMLER Report, Sindelfingen, 2004.
4. Fäult S., Hedin J., Larsson J., Oliveira N., Carlsson B., *Inflateable Side Impact Beams in Martensitic Steel*, SAE International Technical Papers, 2011.
5. Durães M., Peixinho N., *Dynamic Material Properties of Stainless Steel and Multiphase High Strength Steels*, Materials Science Forum, **587–588**, 941–945, 2008.
6. Livermore Software Technology Corporation, "LS-DYNA keywords user's manual", volume I, Version 971, 2007.

Received February 21, 2013; revised version April 26, 2013.

ENGINEERING TRANSACTIONS • *Engng. Trans.* • **61**, 3, 197–218, 2013
Polish Academy of Sciences • Institute of Fundamental Technological Research (IPPT PAN)
National Engineering School of Metz (ENIM)

The Structure Analysis of Secondary (Recycled) AlSi9Cu3 Cast Alloy with and without Heat Treatment

Lenka HURTALOVÁ, Eva TILLOVÁ, Mária CHALUPOVÁ

University of Žilina
Faculty of Mechanical Engineering, Department of Material Engineering
Univerzitná 1, 010 26 Žilina, Slovakia
e-mail: lenka.hurtalova@fstroj.uniza.sk

Al-Si alloys are very universal materials, comprising of from 85% to 90% of the aluminium cast parts produced for the automotive industry (e.g. various motor mounts, engine parts, cylinder heads, pistons, valve retainer, compressor parts, etc.). Production of primary Al- alloys belong to heavy source fouling of life environs. Care of environment of aluminium is connected to the decreasing consumption of resource as energy, materials, water, and soil, and with an increase in recycling and extension life of products in industry. Recycled (secondary) aluminium alloys are made out of Al-scrap and workable Al-garbage by recycling. The automotive casts from aluminium alloys are heat treated for achieving better properties. Al-Si alloys contain more addition elements, that form various intermetallic phases in the structure. They usually contain a certain amount of Fe, Mn, Mg, and Zn that are present either unintentionally, or they are added deliberately to provide special material properties. These elements partly go into the solid solution in the matrix and partly form intermetallic particles during solidification which affect the mechanical properties. Controlling the microstructure of secondary aluminium cast alloy is therefore very important.

Key words: secondary Al alloy, intermetallic phases, structural analysis, solution treatment, mechanical properties.

1. Introduction

The characteristic properties of aluminium, good formability, good corrosion resistance, high strength stiffness to weight ratio, and recycling possibilities make it as the ideal material to replace heavier materials (steel, cast iron or copper) in the car [1]. More than half aluminium on the present produce in European Union comes from recycled raw material. The primary aluminium production needs a lot of energy and constraints decision mining of bauxite. The European Union has big interest of share recycling aluminium and therefore increases interest about secondary aluminium alloys and cast stock from them [2].

The replacement of primary aluminium with recycled has in recent years increasing tendency. The recycled metal is a positive trend, because secondary aluminium produced from recycled metal requires only about 2.8 kWh/kg of metal produced while primary aluminium production requires about 45 kWh/kg produced. The remelting of recycled metal saves almost 95% of the energy needed to produce primary aluminium from ore, and, thus, triggers associated reductions in pollution and greenhouse emissions from mining, ore refining, and melting. Increasing the use of recycled metal is also quite important from an ecological standpoint, since producing Al by recycling creates only about 5% as much CO_2 as by primary production [3].

Due to the increasing utilization of recycled aluminium cast alloys, the quality of recycled Al-Si casting alloys is considered to be a key factor in selecting an alloy casting for a particular engineering application. The mechanical properties will be radically increasing by implementing adaptable alloying- and process technology, leading to larger application fields of complex cast aluminium components such as safety details. Generally, the mechanical and microstructural properties of aluminium cast alloys are dependent on the composition; melt treatment conditions, solidification rate, casting process and the applied thermal treatment [4, 5]. The mechanical properties of Al-Si alloys depend, besides the Si, Cu, Mg and Fe-content, more on the distribution and the shape of the silicon particles [6]. The presence of additional elements in the Al-Si alloys allows many complex intermetallic phases to form, such as binary phases (e.g. Mg_2Si, Al_2Cu), ternary phases (e.g. β-Al_5FeSi, Al_2CuMg, AlFeMn, $A_{17}Cu_4Ni$ and AlFeNi) and quaternary phases (e.g. cubic α-$Al_{15}(FeMn)_3Si_2$ and $Al_{15}Cu_2Mg_8Si_6$) [5, 6–10], all of which may have some solubility for additional elements.

In AlSiCu cast alloy can form these intermetallic phases:

- *Fe-rich intermetallic phases* – Al_5FeSi and $Al_{15}(FeMn)_3Si_2$. The dominant phase is phase know as beta- or β-needles phase Al_5FeSi. This needle-shape phase is more unwanted; because can bring high stress concentrations, thereby increase crack imitation and decreasing the ductility [11, 12]. The deleterious effect of Al_5FeSi can be reduced by increasing the cooling rate or superheating the molten metal. Another way that might by use to suppress the formation this monoclinic phase is converting the morphology by the addition of a suitable "neutralizer" like Mn, Co, Cr, Ni, V, Mo and Be. The most common addition has been Mn. Excess Mn may reduce Al_5FeSi phase and promote formation Fe-rich phases $Al_{15}(FeMn)_3Si_2$ (know as alpha- or α-phase) in form "skeleton like" or in form "Chinese script". This phase has according to some author's cubic or hexagonal structure. If Mg is also present with Si can phase called as pi- or π-phase form – $Al_5Si_6Mg_8Fe_2$. $Al_5Si_6Mg_8Fe_2$ has script-like morphology [11–13].

- *Cu-rich intermetallic phases* – Al_2Cu, Al-Al_2Cu-Si and $Al_5Mg_8Cu_2Si_6$ [11–14]. In unmodified alloys copper is present primarily as Al_2Cu or Al-Al_2Cu-Si phase, in modified alloys as $Al_5Mg_8Cu_2Si_6$. The average size of the copper phase decreases upon Sr modification. The Al_2Cu phase is often observed to precipitate both in a small blocky shape with microhardness 185 HV 0.01. Al-Al_2Cu-Si phase is observed in very fine multi-phase eutectic-like deposits with microhardness 280 HV 0.01 [5, 11, 14, 15].

Influence of intermetallic phases to mechanical and fatigue properties depends on size, volume and morphology these phases [16]. The formation of these phases should correspond to successive reactions during solidification with an increasing number of phases involved at decreasing temperature. In practice, Bäckerud *et al.* [17] identified five reactions in Al-Si-Cu alloy:

609°C: α-dendritic network;

590°C: Liq. $\rightarrow$ α-phase + $Al_{15}Mn_3Si_2$ + Al_5FeSi;

575°C: Liq. $\rightarrow$ α-phase + Si + Al_5FeSi;

525°C: Liq. $\rightarrow$ α-phase + Al_2Cu + Al_5FeSi + Si;

507°C: Liq. $\rightarrow$ α-phase + Al_2Cu + Si + $Al_5Mg_8Si_6Cu_2$.

The quality and the tolerances of compositional secondary alloys are very important, therefore are still under investigation of many academicals and industrial projects. The purpose of the present article is to investigate microstructure of cast Al-Si alloy (without and with heat treatment) prepared by recycling with combination different analytical techniques (light microscopy upon black-white, scanning electron microscopy (SEM) upon deep etching and energy dispersive X-ray analysis (EDX)). As well as changes of the mechanical properties, which are depending on the microstructure changes.

2. Experimental work

For investigation a microstructure was used the AlSi9Cu3 cast alloy with chemical composition 9.4% Si, 2.4% Cu, 0.9% Fe, 0.28% Mg, 0.24% Mn, 1.0% Zn, 0.03% Sn, 0.09% Pb, 0.04% Ti, 0.05% Ni, 0.04% Cr (wt. %). The chemical analysis of cast alloy was carried out using an arc spark spectroscopy. The experimental alloy (prepared by recycling of aluminium scrap) was received in the form of 12.5 kg ingots. Experimental material was molten into the chill mould (chill casting) (Fig. 1). The melting temperature was maintained at 760°C ±5°C. Molten metal was purified with salt AlCu4B6 before casting and was not modified or grain refined.

a)

b)

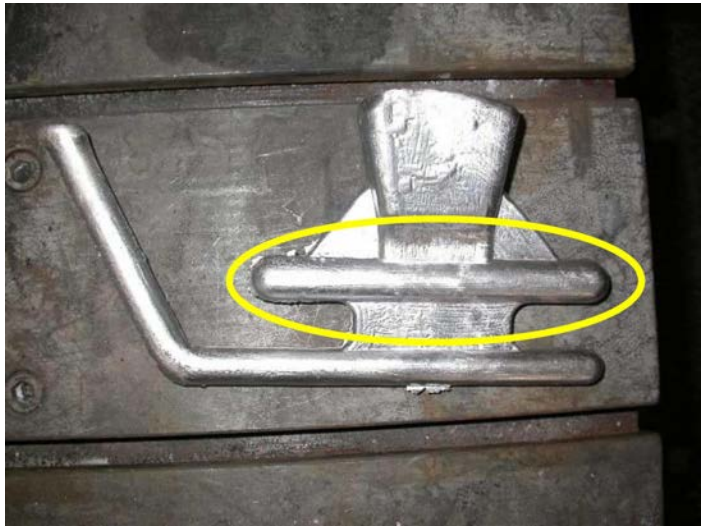

FIG. 1. Metallic mould and molten semi-product: a) metallic mould with semi-product, b) detail of semi-product.

AlSi9Cu3 cast alloy has lower corrosion resistance and is suitable for high temperature applications (dynamic exposed casts, where are not so big requirements on mechanical properties) – it means to max. 250°C. The AlSi9Cu3 alloy has these technological properties: tensile strength (R_m = 240–310 MPa), offset 0.2% yield stress ($R_p0.2$ = 140–240 MPa), however the low ductility limits (A_5 = 0.5–3%) and hardness HB 80–120 [18, 19].

Microstructural characterization was performed using light microscope Neophot 32 and SEM observation with EDX analysis using scanning electron microscope VEGA LMU II, while phase microanalysis was performed using energy dispersive X ray spectroscopy EDX (EDX analyzer Brucker Quantax). The samples for metallographic observations (1.5×1.5 cm) were prepared by standards metallographic procedures (wet ground, polished with diamond pastes, finally polished with commercial fine silica slurry – STRUERS OP-U and etched by standard reagent (Dix-Keller, 0.5% HF). Some samples were also deep-etched in order to reveal the three-dimensional morphology of the silicon phase and intermetallic phases for 30 s in HCl solution. The specimen preparation procedure for deep-etching consists of dissolving the aluminium matrix in a reagent that will not attack the eutectic components or intermetallic phases. The residuals of the etching products should be removed by intensive rinsing in alcohol. The preliminary preparation of the specimen is not necessary, but removing the superficial deformed or contaminated layer can shorten the process. Same pictures were made with using backscattered electrons. The backscattered electrons are beam electrons that are reflected from the sample by elastic scattering. BSE are often used in analytical SEM, because the intensity of the BSE signal is strongly related to the atomic number of the specimen, BSE images can provide information about the distribution of different elements in the sample [16].

For better mechanical properties of Al-Si alloys is good to use a heat treatment. Mechanical and fatigue properties of aluminium cast depends on size, volume and morphology of intermetallic phases and silicon particles [16]. During heat treatment the morphology of intermetallic phases and silicon particles was change and therefore was use solution treatment of AlSi9Cu3 alloy. Heat treatment consist of solution treatment at temperature 505, 515 and 525°C with holding time 2, 4, 8, 16 and 32 hours, than water quenching at 40°C and nature aging for 24 hours on air.

3. Results of experimental work

AlSi9Cu3 belongs to hypoeutectic aluminium cast alloys because contains 9.4% of Si. The Fig. 2 shows as-cast microstructure of the experimental secondary AlSi9Cu3 cast alloy. The analyzed microstructure contains primary aluminium dendrites (α-phase – light grey – 1), eutectic (mixture of α-matrix and spherical dark grey Si-particles – 2) and variously type's Cu- and Fe-rich intermetallic phases (3, 4), that are concentrated mainly in the interdendritic spaces. In view of the grey scale values in the SEM secondary electron images are higher (brighter) for the higher atomic number of the elements, phases containing Cu and/or Fe are brightest (Fig. 2b).

a) etch. Dix-Keller

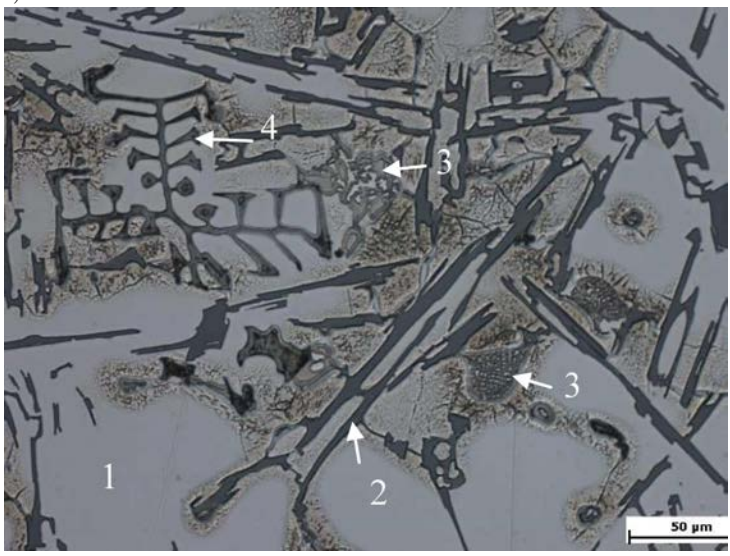

b) deep-etch., SEM, BSE

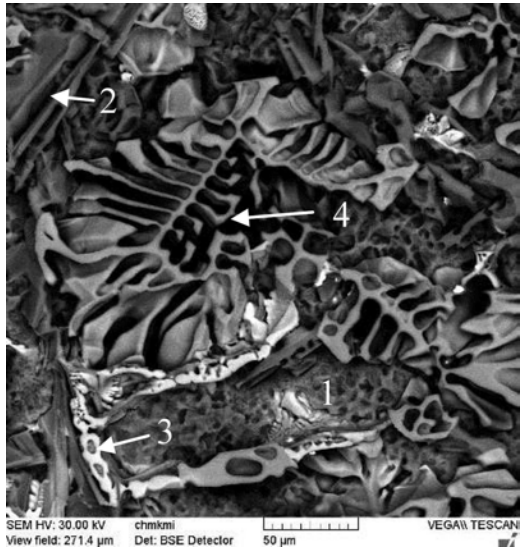

FIG. 2. Microstructure of AlSi9Cu3 cast alloy.

3.1. Eutectic and eutectic silicon

The eutectic is mixture of α-matrix and Si particles. The α-matrix precipitates from the liquid as the primary phase in the form of dendrites and is comprised of Al and Si (Fig. 2, Fig. 3a). Silicon is an anisotropic phase.

a) α-phase

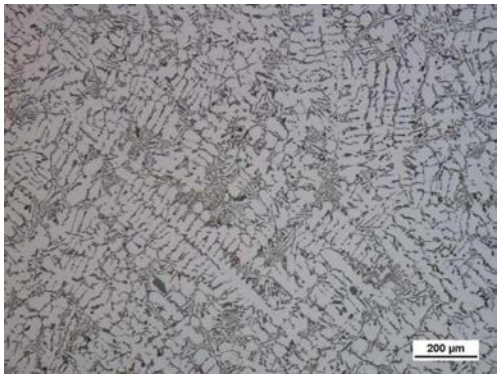

etch. Dix-Keller

b) eutectic Si

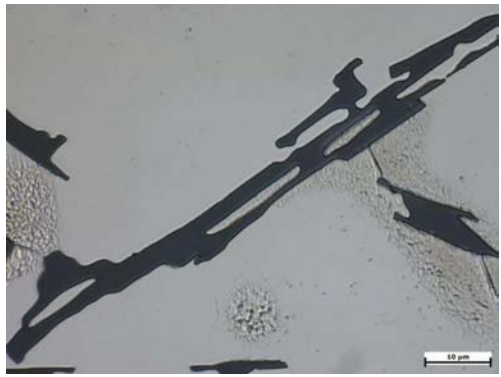

etch. Dix-Keller

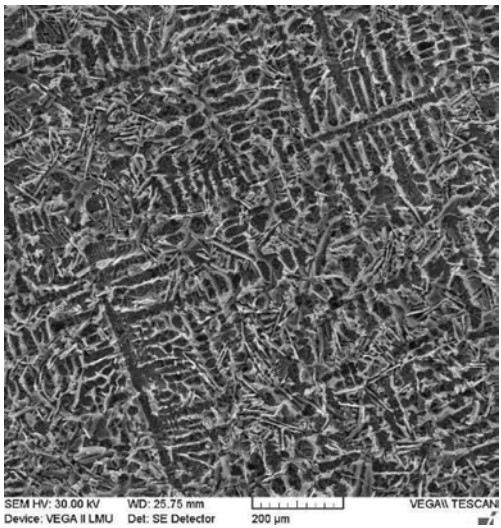

deep etch. HCl, SEM

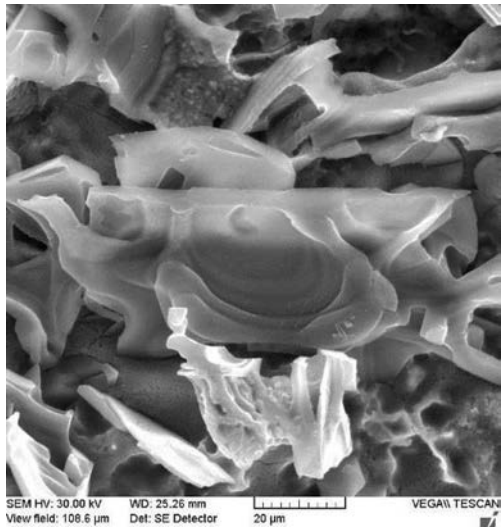

deep etch. HCl., SEM

FIG. 3. Eutectic and eutectic Si in as-cast structure of AlSi9Cu3 cast alloy.

Experimental material was not grain refined and not modified so eutectic Si grows in a faceted manner along preferred crystallographic directions according to the twin plane re-entrant edge mechanism (TPRE-mechanism) as platelets (Fig. 3b). Most likely Si-platelets grew epitaxial from the surrounding primary aluminium dendrites. This result is in accordance with reports for unmodified Al-Si alloys.

a) 505°C/4 h

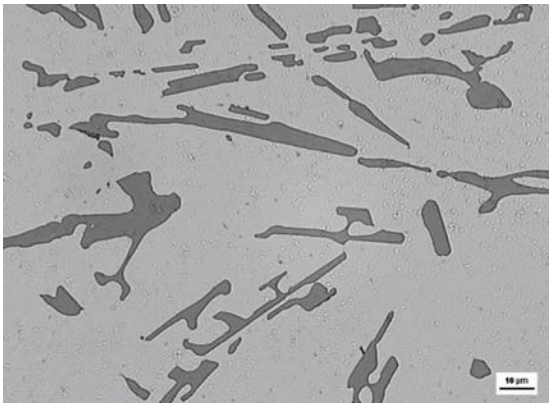

etch. Dix-Keller

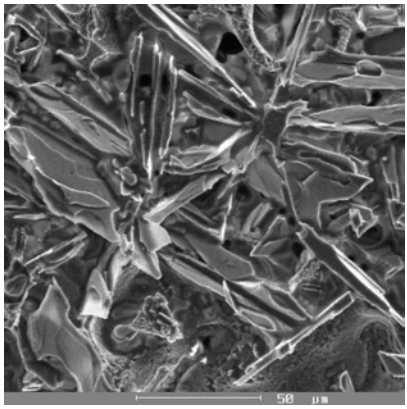

deep etch. HCl., SEM

b) 515°C/4 h

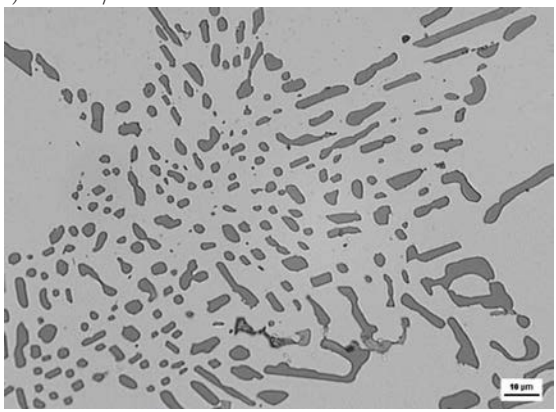

etch. Dix-Keller

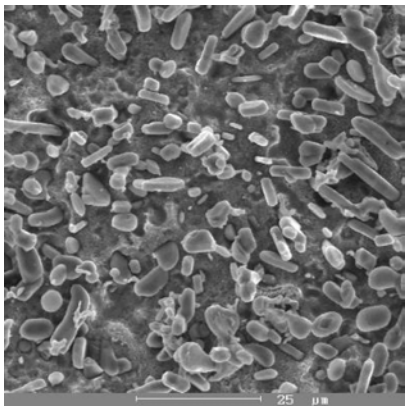

deep etch. HCl., SEM

c) 525°C/4 h

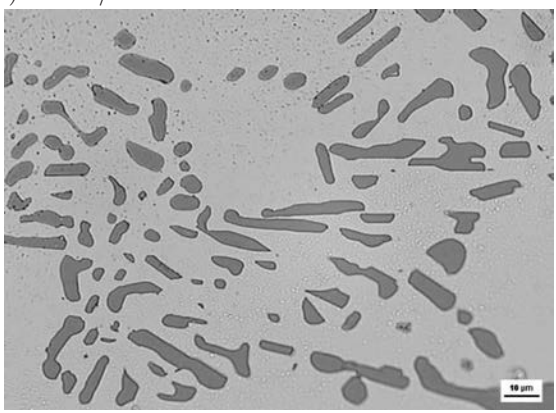

etch. Dix-Keller

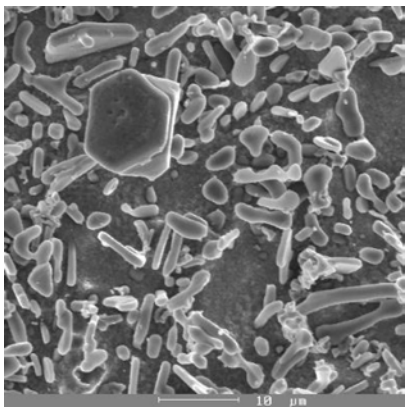

deep etch. HCl., SEM

Fig. 4. Eutectic Si after heat treatment of AlSi9Cu3 cast alloy.

The mechanical properties of cast component are determined largely by the shape and distribution of Si particles and intermetallic phases in α-matrix. This plate-like type of morphology of eutectic Si is not good for mechanical properties, because Si platelets are hard but brittle and can crack exposing the soft α-matrix. Therefore are needs to affect this morphology with the appropriate manner. The kinetics of Si morphology transformation is influencing with the solution treatment (under certain conditions). Heat treatment affects the precipitates size, shape and distribution in a cast component too [20]. The spheroidization process of Si particles takes place in two stages with application of solution treatment: a) fragmentation or dissolution of the eutectic Si branches; b) spheroidization of the separated branches [21, 22]. Optimum tensile, impact and fatigue properties are obtained with small, spherical and evenly distributed particles. Silicon also imparts heat treating ability to the casting through the formation of compounds with Mg, Fe and Cu. For that reason the AlSi9Cu3 cast alloy was heat treated.

The effect of solution treatment on morphology of eutectic Si is demonstrated in Fig. 4. The changes in morphology of eutectic Si observed after heat treatments are documented for holding time of 4 hours. Eutectic Si without heat treatment (untreated state) occurs in platelets form (Fig. 3b). After solution treatment by temperature of 505°C we noted that the platelets were fragmentized into smaller platelets with spherical edges (Fig. 4a). The spheroidized process dominated at 515°C. The smaller Si particles were spheroidized to rounded shape, see Fig. 4b. By solution treatment at 525°C the spheroidized particles gradually grew larger (coarsening) (Fig. 4c).

3.2. Fe-rich intermetallic phases

Iron is one of the most critical alloying elements, because Fe is the most common and usually detrimental impurity in cast Al-Si alloys. The Fe impurity in Al-Si cast alloys results mainly from the use of steel tools and scrap materials [10, 12, 23].

The solubility of iron is very low in aluminium alloys so most iron forms intermetallic phases. According to [24], the two main types of Fe-rich intermetallic phases occurring in this AlSi9Cu3 alloy are Al_5FeSi and $Al_{15}(FeMn)_3Si_2$. Significant levels of Fe (e.g. $> 0.5\%$) can change the solidification characteristics of Al-Si alloys by forming pre- and post-eutectic Al_5FeSi phase [6, 11]. Al_5FeSi phases precipitate in the interdendritic and intergranular regions as platelets (appearing as needles in the metallographic microscope – Fig. 5a). Long and brittle Al_5FeSi platelets (more than 500 μm) can adversely affect mechanical properties and also lead to the formation of excessive shrinkage porosity de-

a) Al_5FeSi b) $Al_{15}(FeMn)_3Si_2$

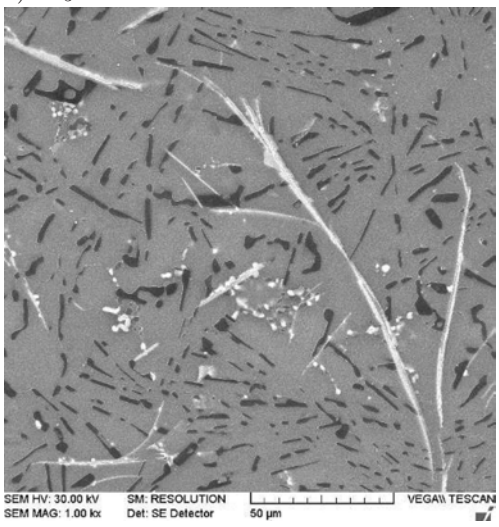

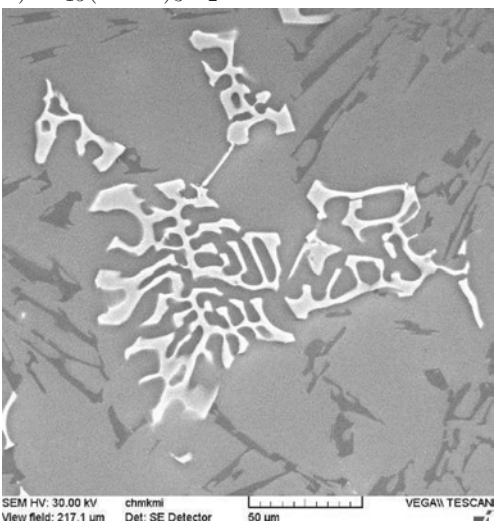

etch. 0.5 HF etch. 0.5 HF

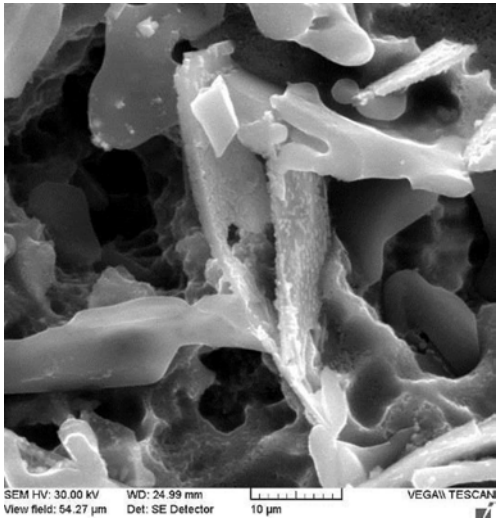

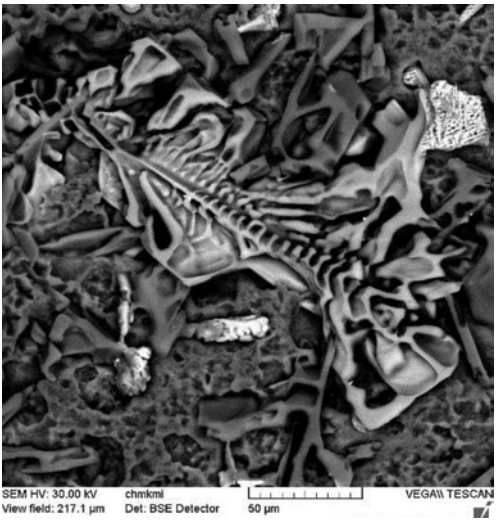

deep etch. HCl deep etch. HCl, BSE

FIG. 5. Morphology of Fe-rich intermetallic phases in as-cast structure of AlSi9Cu3 cast alloy, SEM.

fects in castings [25]. TAYLOR [11] further suggested that the formation of large β platelets at high Fe-contents facilitates the nucleation of eutectic Si, therefore leading to a rapid deterioration of the interdendritic permeability. The β platelets appeared to be the main nucleation sites for the eutectic Si and Cu-rich

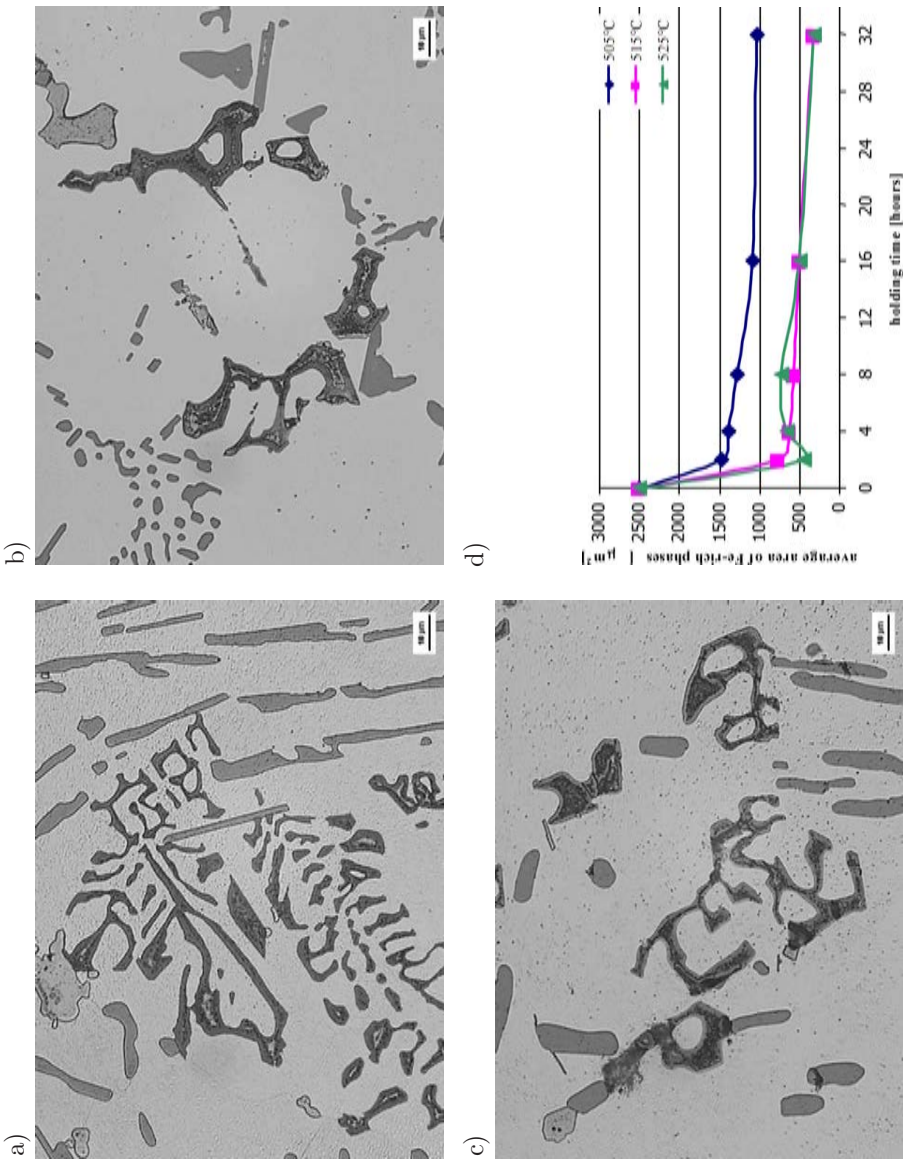

FIG. 6. Effect of heat treatment on Fe-rich phases of AlSi9Cu3 cast alloy: a) 505°C/4 h, etch. Dix-Keller, b) 515°C/4 h, etch. Dix-Keller, c) 525°C/4 h, etch. Dix-Keller, d) changes in average area of Fe-rich phases.

phase. Nucleation of Si and Al_2Cu may occur on large Al_5FeSi platelets. Phase with cubic crystal structure – $Al_{15}(FeMn)_3Si_2$ is considered less harmful to the mechanical properties than β phase [26, 27]. This phase (Fig. 5b) has a compact morphology "Chinese script" or skeleton-like, which does not initiate cracks in the cast material to the same extent as the Al_5FeSi (Fig. 5a).

The Fe-rich particles can be twice as large as the Si particles, and the cooling rate has a direct impact on the kinetics, quantities and size of Fe-rich intermetallic present in the microstructure. In experimental recycled AlSi9Cu3 cast alloy that contains less than 0.9% of Fe and 0.24% of Mn were observed Al_5FeSi needles (Fig. 5a) – on deep etcher samples plate-like form (Fig. 5a) and $Al_{15}(FeMn)_3Si_2$ – skeleton-like form (Fig. 5b). In experimental material was satisfied condition $Fe : Mn = 2 : 1$, therefore intermetallic needles phases were observed in a few isolated cases.

Heat treatment was use for affecting the size of Fe-rich phases, because the shape and size of iron compounds is more influential than the quantity of those iron compounds. The evolution of the Fe-rich phases during solution treatment is described in Fig. 6. Al_5FeSi phase is dissolved into very small needles (difficult to observe). The $Al_{15}(MnFe)_3Si_2$ phase was fragmented to smaller skeleton particles. In the untreated state $Al_{15}(FeMn)_3Si_2$ phase has a compact skeleton-like form (Fig. 5b). Solution treatment of this skeleton-like phase at 505°C tends to fragmentation (Fig. 6a) and at 515 or 525°C to spheroidization and segmentation (Fig. 6b, c).

For the confirmation that solution treatment reduces Fe-rich phases area and affects its morphology was used the quantitative metallography. Quantitative metallography was carried out on an Image Analyzer NIS – Elements to quantify Fe-rich phases (average area) morphology changes, during solution treatment. Figure 6d shows the changes in the average area of Fe-rich phases during solution treatment. The maximum average area of Fe-rich phases was observed in as-cast samples (2 495 μm^2). By increasing the solution temperature the average area of Fe-phases drop to (the increasing temperature of solution treatment causes dropping the average area of Fe-phases to 320 μm^2 by 515°C). With a prolonged solution treatment time more than 8 h, the extent of dissolution of Fe-rich phases changed little.

3.3. Cu-rich intermetallic phases

Half or more of the copper is found as a component of intermetallic compounds [28]. Cu intermetallic phases are in aluminium alloys forming such as Al_2Cu with tetragonal crystal structure, which solidified in two morphologies after Al-Si eutectic reaction. The first are as massive or blocky form (Al_2Cu

– Fig. 7a-1, 7c) with high copper concentration ∼38–40 % Cu and second are as fine ternary eutectic form (Al-Al_2Cu-Si – Fig. 7a-2, 7b, 7d). The latter type is more pronounced in the unmodified alloy and was observed either as separate eutectic pockets or precipitated on pre-existing Si-particles or Fe-phases [26, 28, 29]. In experimental material were observed both types of Cu-rich intermetallic phases (Fig. 7).

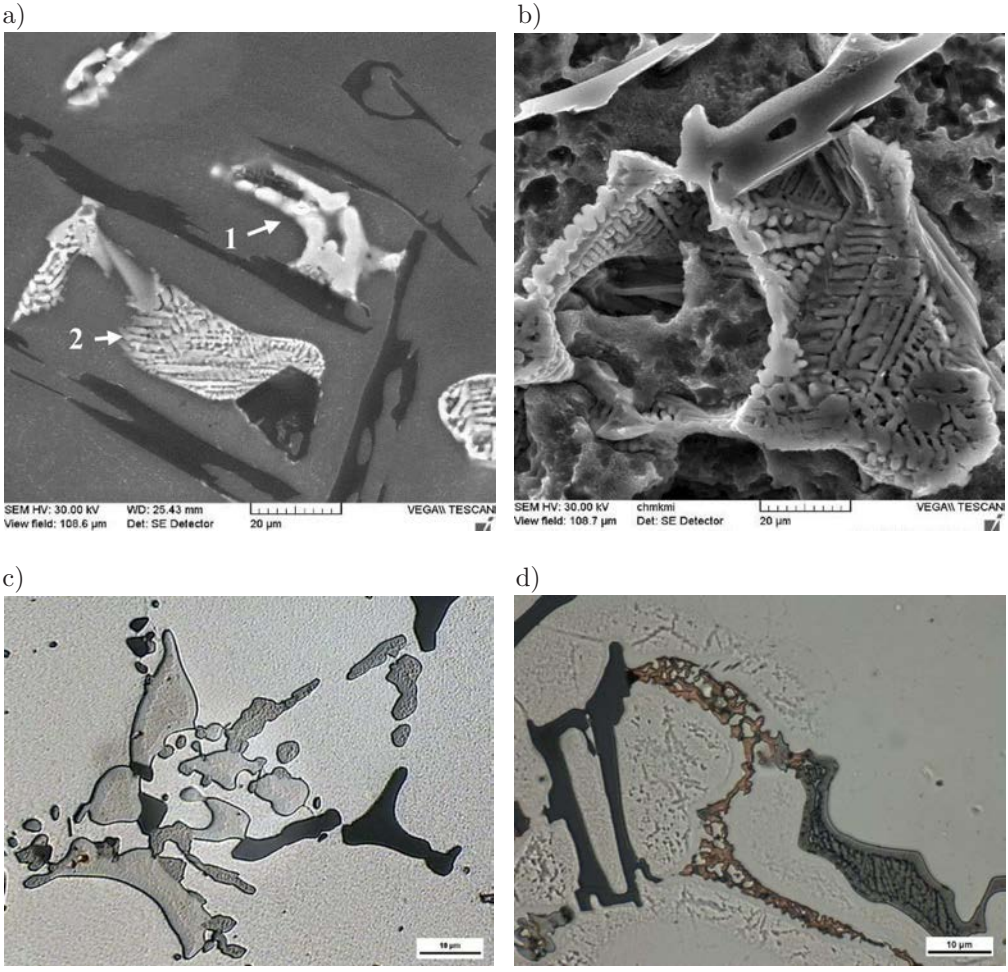

Fig. 7. Morphology of Cu-rich intermetallic phases in as-cast structure of AlSi9Cu3 cast alloy: a) 1-Al_2Cu, 2- Al-Al_2Cu-Si, etch. Dix-Keller, SEM, b) Al-Al_2Cu-Si, deep etch. HCl, SEM, c) detail of Al_2Cu phase, etch. Dix-Keller, d) detail of Al-Al_2Cu-Si phase, etch. Dix-Keller.

The increasing level of Cu improves the strength of the aluminium alloy through the formation of Cu based precipitate during heat treatment. The effect of heat treatment on morphology of Cu-rich phases was followed by optical and

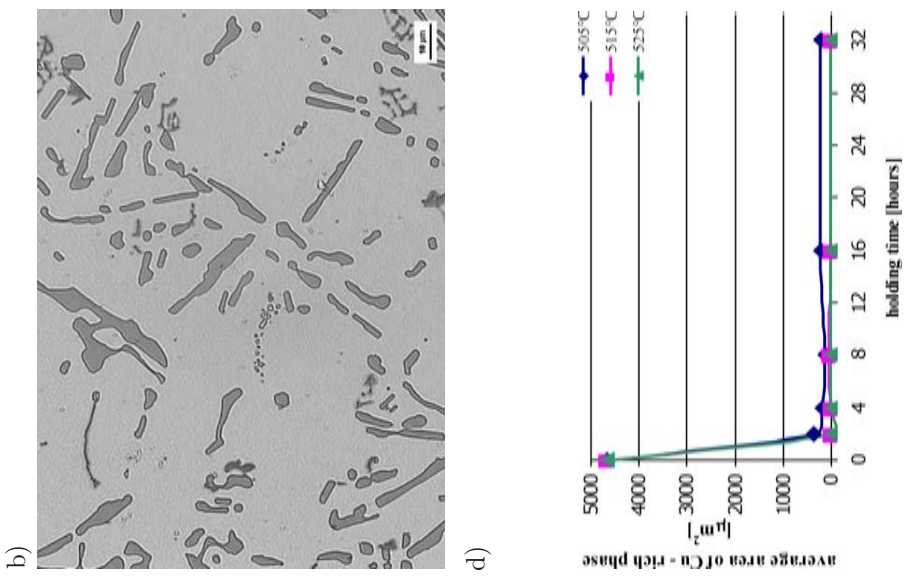

FIG. 8. Effect of heat treatment on Cu-rich phases of AlSi9Cu3 cast alloy: a) 505°C/4 h, etch. Dix-Keller, b) 515°C/4 h, etch. Dix-Keller, c) 525°C/4 h, etch. Dix-Keller, d) changes in average area of Cu-rich phases.

electron microscopy. Morphology changes of Al-Al_2Cu-Si during heat treatment are demonstrated in Fig. 8. The changes of morphology of Al-Al_2Cu-Si observed after heat treatment are documented for holding time 4 hours.

Al-Al_2Cu-Si phase without heat treatment (as-cast state) occurs in form compact oval troops (Fig. 7). After solution treatment at temperature 505°C these phase disintegrated into smaller segments. The amount of Al-Al_2Cu-Si phase decreases. This phase is gradually dissolved into the surrounding Al-matrix with an increase in solution treatment time (Fig. 8a). By solution treatment 515°C was this phase observed in the form coarsened globular particles and these occurs along the black needles, probably Fe-rich Al_5FeSi phase (Fig. 8b). By solution treatment 525°C was this phase documented in the form molten particles with homogenous shape (Fig. 8c).

The changes of average area of Cu rich phases were confirmed by using the quantitative metallography, too. Figure 8d shows average area of Cu-rich phases obtained in solution heat treated samples. Maximum average area of Al-Al_2Cu-Si phase was observed by temperature solution treatment at 505°C with holding times 2 hours (357 μm^2). Minimum average area of Al-Al_2Cu-Si phase particle was observed by temperature solution treatment at 515°C (0.277 μm^2). It is evident that heating at temperatures below the final solidification temperature (505°C, 515°C and 525°C) results in dissolution of Al-Al_2Cu-Si phase [29–31]. Solution treatment at 525°C apparently causes a marked change (Fig. 8). This, however, is attributed to the melting of the Al-Al_2Cu-Si, rather than to its dissolution. Dissolution and melting of Al_2Cu phase in AlSi9Cu3 alloy has been studied in detail by Samuel [32]. When the AlSi9Cu3 alloy is solution treated at temperature about the melting point of the eutectic (Al+Al_2Cu) phase, e.g. 525–540°C, the Al-Al_2Cu-Si particles may undergo incipient melting even after periods as 4 hours [29–31].

3.4. SEM image and X-ray analysis

The SEM image and X-rays analysis were used for a complete structural analysis of experimental material. Figure 9 shows typical example: a SEM image and X-rays analysis of Al-Al_2Cu-Si.

Structural analysis identified of recycled (secondary) AlSi9Cu3 cast alloy as basic structural elements: α-phase, Si platelets, Fe-rich intermetallic phases: needles – Al_5FeSi (but in a small volume); skeleton-like $Al_{15}(FeMn)_3Si_2$ phase and Cu-rich intermetallic phase: Al_2Cu (but in a small volume); Al-Al_2Cu-Si ternary eutectic. The EDX analysis revealed that the identified Cu-rich and Fe-rich intermetallic phases by using light microscopy are really these intermetallic phases, because chemical composition of these phases was confirmed by EDX analysis.

a)

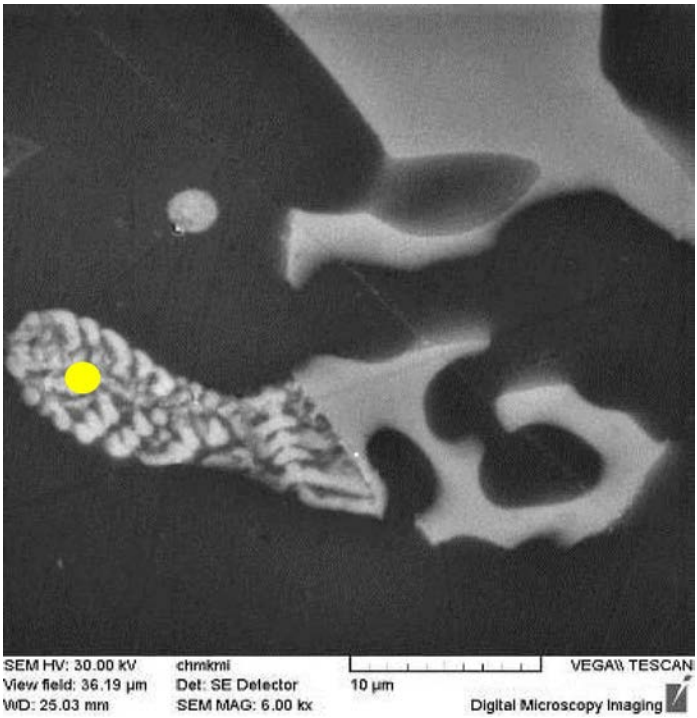
SEM HV: 30.00 kV
View field: 36.19 µm
WD: 25.03 mm
chmkmi
Det: SE Detector
SEM MAG: 6.00 kx
10 µm
VEGA\\ TESCAN
Digital Microscopy Imaging

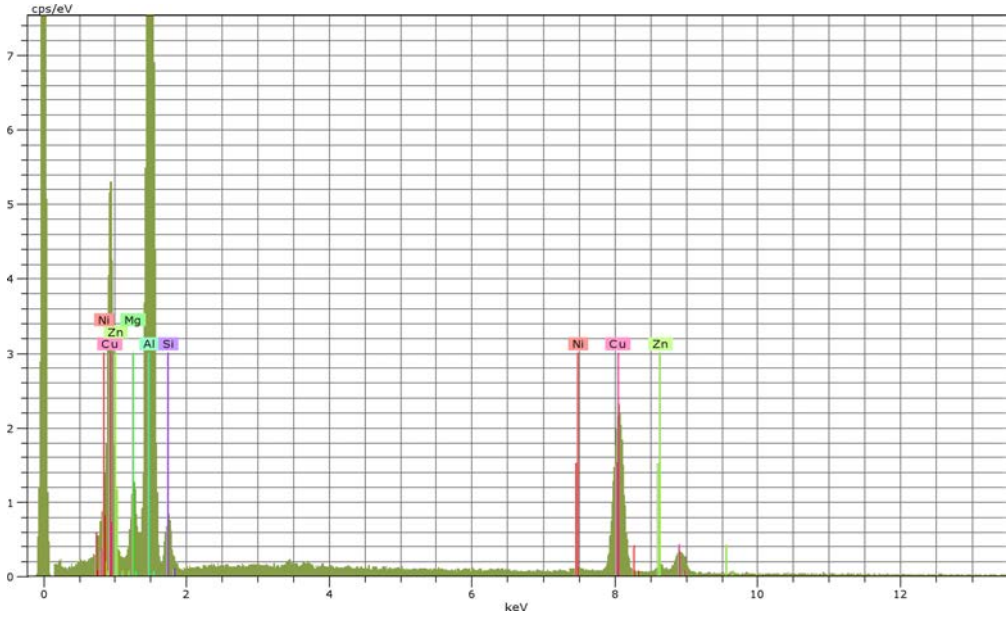
cps/eV
keV
Ni
Mg
Zn
Cu
Al
Si
Ni
Cu
Zn

[Fig. 9]

b)

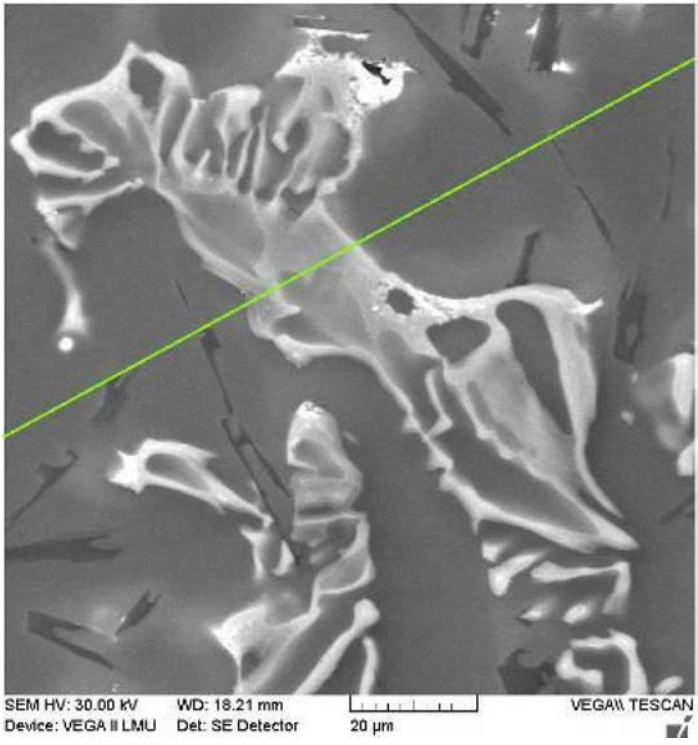
SEM HV: 30.00 kV
WD: 18.21 mm
VEGA\\ TESCAN
Device: VEGA II LMU
Det: SE Detector
20 µm

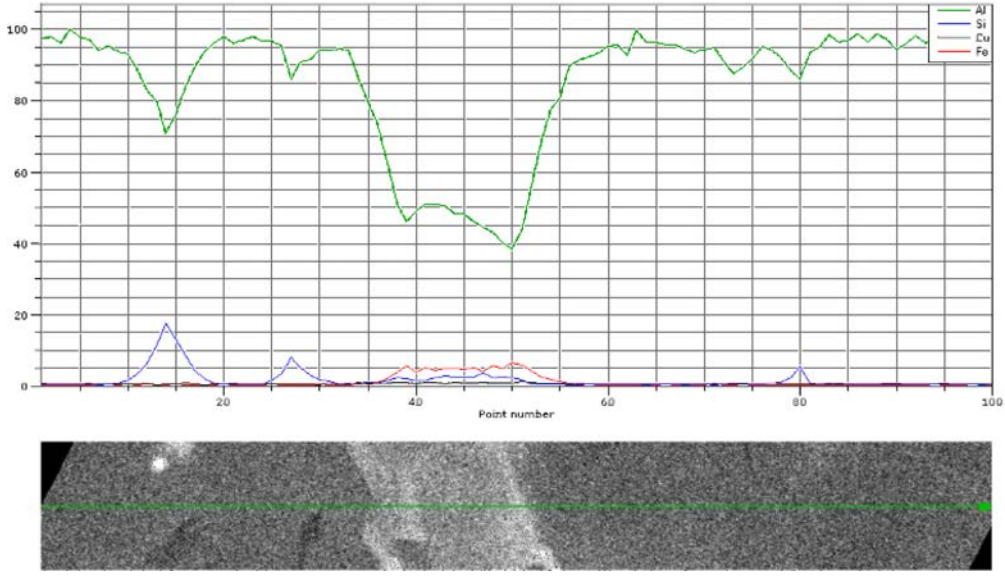
Al
Si
Cu
Fe
100
80
60
40
20
0
20
40
60
80
100
Point number

[Fig. 9]

c)

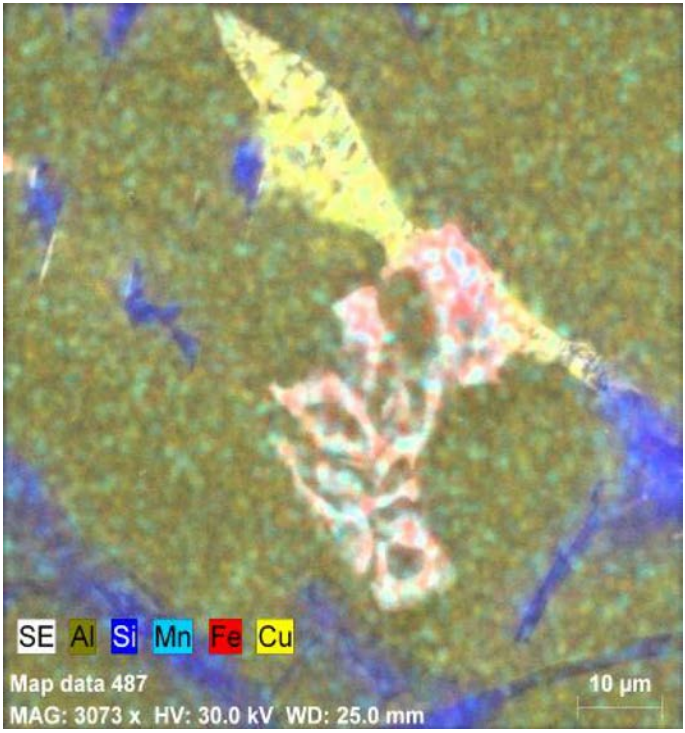

FIG. 9. Analysis of intermetallic phases in as-cast state of AlSi9Cu3 cast alloy, SEM: a) point X-ray analysis, b) line X-ray analysis, c) SEM image analysis.

3.5. Changes of mechanical properties causes with changes of structure

Heat treatment is one of the major factors used to enhance the mechanical properties of heat-treatable Al-Si alloys, through an optimization of both solution and aging heat treatments. The solution treatment homogenises the cast structure and minimizes segregation of alloying elements in the casting. Segregation of solute elements resulting from dendritic solidification may have an adverse effect on mechanical properties.

Changes of microstructural parameters cause changes in mechanical properties during solution treatment. Solution treatment performs tree roles: homogenization of as-cast structure; dissolution of certain intermetallic phases such as Al_2Cu; changes the morphology of eutectic Si and intermetallic phases by fragmentation, spheroidization and coarsening, thereby improving mechanical properties.

After heat treatment were samples subjected for mechanical test (strength tensile and Brinell hardness). Influence of solution treatment and changes of microstructural parameters on mechanical properties are shown on Fig. 10 and

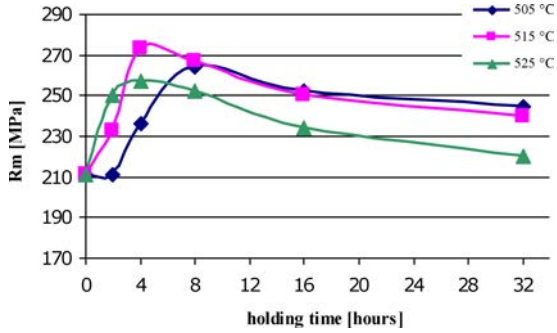

FIG. 10. Changes of strength tensile.

Fig. 11. After solution treatment tensile strength and hardness are remarkably improved, compared to the corresponding as-cast condition. Highest strength tensile was 273 MPa for 515°C/4 hours (Fig. 10). With further increase in solution temperature more than 515°C and solution time more than 8 hours, tensile strength gently decreases during the whole solution period.

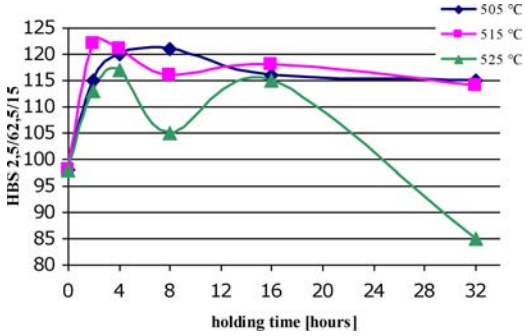

FIG. 11. Changes of Brinell hardness.

Results of hardness (Fig. 11) are comparable with results of tensile strength. Highest hardness was 124 HBS for 515°C/2 hours. The hardness decreases during the temperature 525°C due to melting of the Al-Al_2Cu-Si phase by this temperature [29–31].

4. Conclusion

Understanding metal quality is of great importance for control and prediction of casting characteristics. The results of optical and SEM studies of recycled (secondary) AlSi9Cu3 cast alloy are summarized as follows:

- Structural analysis identified as basic structural elements: α-phase, Si platelets, and intermetallic phases ($Al_{15}(FeMn)_3Si_2$ in the skeleton-like form, Al_5FeSi

in form needles and Cu-ternary eutectic Al-Al_2Cu-Si, Al_2Cu in a small block shape).

- In experimental material are dominant: Cu-rich phase Al-Al_2Cu-Si and Fe-phases $Al_{15}(FeMn)_3Si_2$ (thanks to the presence of Mn). Chemical composition of all phases was confirmed by EDX analysis.
- During heat treatment Si particles spheroidized. As the optimum temperature of spheroidization the eutectic Si was specified the temperature 515°C.
- The morphology and size of iron phases are highly dependent on the solution treatment. Platelets Fe-rich phases (Al_5FeSi) are dissolved into very small needle phases. Skeleton-like Fe-rich phases ($Al_{15}(FeMn)_3Si_2$) are fragmented and dissolved (average area reduces from 2 495 to 320 μm^2).
- Al-Al_2Cu-Si phases are fragmented, dissolved and redistributed within α-matrix (average area of Cu-phases particle decreases from 9 995.5 μm^2 to 0.277 μm^2) during heat treatment.
- Changes of microstructural parameters of AlSi9Cu3 cause changes in mechanical properties. The highest strength tensile was at a temperature of 515°C with holding time 4 hours; the highest hardness at a temperature of 515°C with holding time 2 and 4 hours. For this was defined as optimum regime of solution treatment for experimental samples from AlSi9Cu3 cast alloy using in automotive industries regime: 515°C with a holding time of 4 hours, water quenching at 40°C and nature aging for 24 hours on air. After heat treatment, casts for automotive industries have better mechanical properties as in an as-cast state.

Acknowledgment

The authors acknowledge the financial support of the projects No. 1/0841/11 and No. 1/0460/11.

References

1. Miller W.S., Zhuang L., Bottema J. *et al.*, *Recent development in aluminium alloys for the automotive industry*, Materials Science and Engineering, **A 280**, 37–49, 2000.
2. Senčáková L., Virčíková E., *Life cycle assessment of primary aluminium production*, Acta Metallurgica Slovaca, **13**, 3, 412–419, 2007.
3. Das K.S., *Designing Aluminum Alloys for a Recycling Friendly World*, Materials Science Forum, **519–521**, 1239–1244, 2006.
4. Michna Š., Lukáč I., Očenášek V., Kořený R., Drápala J., Schneider H., Miškufová A., *Encyclopedia of aluminium* [in Czech: *Encyklopédia hliníku*], Adin, s.r.o. Prešov – Slovakia, 2005.
5. Tillová E., Chalupová M., *Structural analysis of Al-Si cast alloys*, EDIS Žilina, Žilina, Slovakia, 2009 (in Slovak).

6. Seifeddine S., *The influence of Fe on the microstructure and mechanical properties of cast Al-Si alloys*, Literature review – Vilmer project, Jönköping University, Sweden, 2007.

7. Shabestari S.G., *The effect of iron and manganese on the formation of intermetallic compounds in aluminum-silicon alloys*, Materials Science and Engineering A, 383, 289–298, 2004.

8. Samuel A.M., Samuel F.H., *Effect of alloying elements and dendrite arm spacing on the microstructure and hardness of an Al-Si-Cu-Mg-Fe-Mn (380) aluminium die-casting alloy*, Journal of Materials Science, 30, 1698–1708, 1995.

9. Samuel A.M., Samuel F.H., Doty H.W., *Observations on the formation of β-AlFeSi phase in 319 type Al-Si alloys*, Journal of Materials Science, 31, 5529–5539, 1996.

10. Tillová E., Chalupová M., Hurtalová L., *Evolution of the Fe-rich phases in recycled AlSi9Cu3 cast alloy during solution treatment*, Communications – Scientific letters of the university of Žilina, **12**, 4, 95–101, 2010.

11. Taylor J.A., *The effect of iron in Al-Si casting alloys*, 35th Australian Foundry Institute National Conference, Adelaide, South Australia, 148–157, 2004.

12. Seifedine S., Johansson S., Svensson I., *The influence of cooling rate and manganese content on the β-Al_5FeSi phase formation and mechanical properties of Al-Si – based alloys*, Materials Science and Engineering A, 490, 385–390, 2008.

13. Moustafa M.A., *Effect of iron content on the formation of ß-Al_5FeSi and porosity in Al-Si eutectic alloys*, Journal of Materials Processing Technology, 209, 605–610, 2009.

14. Rios C.T., Caram R., *Intermetallic compounds in the Al-Si-Cu system*, Acta Microscopica, **12**, 1, 77–81, 2003.

15. Hurtalová L. *et al.*, *Changes in structural characteristics of hypoeutectic al-Si cast alloy after age hardening*, Materials science (Medžiagotyra), **18**, 3, 228–233, 2012.

16. Tillová E., Chalupová M., Hurtalová L., *Evolution of phases in a recycled Al-Si cast alloy during solution treatment*, The Scaning Electron Microscope, INTECH, 411–438, 2011.

17. Bäckerud L., Chai G., Tamminen J., *Solidification Characteristics of Aluminum Alloys*, Vol. 2, AFS, 1992.

18. www.honsel.com/uploads/media/Handbuch_Gusswerkstoffe.pdf, 12.11.2010, 12:32.

19. www.krdiecasting.com/pdf/Sect3.pdf, 13.01.2011, 14:22.

20. Boileau M.J., Allison J.E., *The effect of solution time and heat treatment on the fatigue properties of a cast 319 aluminium alloy*, Metallurgical and materials transactions A, **34A**, 1807–1820, 2003.

21. Li R., *Solution heat treatment of 354 and 355 cast alloys*, AFS Transaction, 26, 777–783, 1996.

22. Ma Z. *et al.*, *Influence of aging treatments and alloying additives on the hardness of Al-11Si-2.5Cu-Mg alloys*, Materials and Design, **31**, 3791–3803, 2010.

23. Lu L., Dahle A.K., *Iron-Rich Intermetallic Phases and Their Role in Casting Defect Formation in Hypoeutectic Al-Si Alloys*, Metallurgical and Transactions A, **36A**, 819–835J, 2005.

24. Kral M.V., *A crystallographic identification of intermetallic phases in Al-Si alloys,* Materials Letters, 1–6, 2005.

25. Caceres C.H., Svenson I.L., Taylor J.A., *Strenght-ductility Behaviour of Al-Si-Cu-Mg Casting Alloys in T6 temper*, Int. J. Cast Metals Res., 15, 531–543, 2003.

26. Yi J.Z., Gao X.Y., Lee P.D., Lindley T.C., *Effect of Fe-content on fatigue crack initiation and propagation in a cast aluminium - silicon alloy (A356-T6)*, Materials Science and Engineering, **A 386**, 396–407, 2004.

27. Ma Z., Samuel A.M., Samuel F.H., Doty H.W., Valtierra S., *A study of tensile properties in Al-Si-Cu and Al-Si-Mg alloys: Effect of β-iron intermetallics and porosity*, Materials Science and Engineering A, **490**, 36–51, 2008.

28. Dobrzański L.A., Borek W., Maniara R., *Influence of the crystallization condition on Al-Si-Cu casting alloys structure*, Jamme, **18**, 1–2, 211–214, 2006.

29. Hurtalová L., Tillová E., Chalupová M., *Cu-rich intermetallic phases in recycled AlSi9Cu3 cast alloy – a comparison between aging behavior in T4 and T6 treatments*, Perners contacts – Electronical Technical Journal of Technology, Engineering and Logistic in Transport, **VI**, 2, 72–80, 2011.

30. Hurtalová L., Tillová E., *Dissolution and melting of Al_2Cu phase particles in recycled AlSi9Cu3 cast alloy*, Materials Engineering, **XVI**, 3a, 110–115, 2009.

31. Tillová E., Hurtalová L., Chalupová M., *Evolution of Cu-rich phases during solution treatment*, 26th Danubia-Adria symposium on Advances in Experimental Mechanics, Montanuniversität Leoben-Austria, 231–232, 2009.

32. Samuel F.H., *Incipient melting of $Al_5Mg_8Si_6Cu_2$ and Al_2Cu intermetallics in unmodified and strontium-modified Al-Si-Cu-Mg (319) alloys during solution heat treatment*, Journal of Materials Science, **33**, 2283–2297, 1998.

Received February 25, 2013; revised version June 24, 2013.

ENGINEERING TRANSACTIONS • *Engng. Trans.* • **61**, 3, 219–229, 2013
Polish Academy of Sciences • Institute of Fundamental Technological Research (IPPT PAN)
National Engineering School of Metz (ENIM)

Fracture Toughness Investigations of Metal Matrix Composites Using Compact Specimens

Tadeusz SZYMCZAK[1)], Zbigniew L. KOWALEWSKI[1), 2)]

[1)] *Motor Transport Institute*
Centre for Material Testing and Mechatronics
Jagiellońska 80, 03-301 Warsaw, Poland
e-mail: tadeusz.szymczak@its.waw.pl

[2)] *Institute of Fundamental Technological Research PAN*
Department for Strength of Materials
Pawińskiego 5B, 02-106 Warsaw, Poland

This paper presents experimental results of the fracture toughness tests carried out on metal matrix composites. The material was produced using the 44200 aluminium alloy reinforced by Al_2O_3 in the form of Saffil fibres. Three different contents of Al_2O_3 were taken into account, i.e. 10%, 15%, 20%. The main aim of the research was to examine an influence of the aluminium oxide content on a critical value of the stress intensity factor, K_{IC}. All tests were performed using a miniature compact specimen, which was four times smaller than the typical one. The results of FEA analysis confirmed a typical distribution of the effective stress at the tip of the notch. In each test the composite specimen was mounted in the loading system of the testing machine by applying special grips. Crack tip opening displacement of the specimen notch was measured by means of the clip on knife edge extensometer having 10 mm gauge length. The results in form of tensile force versus crack tip opening displacement show the first mode of fracture. An inspection of the pre-cracked zone of the composite did not exhibit the typical features usually observed on specimen surface after fatigue. An influence of the Al_2O_3 Saffil fibres content within the range from 10% to 20% on a critical value of the stress intensity factor was negligible small. The K_{IC} of the composites tested in this research achieved the level of 12 MPa $m^{1/2}$.

Key words: metal matrix composite, fracture toughness test, compact specimen, fatigue zone, stress intensity factor.

1. Introduction

Classification of modern materials for engineering applications requires knowledge about their mechanical parameters. Among many of such parameters one can distinguish: Young's modulus, proportional limit, yield point, ultimate tensile strength, and stress intensity factor (SIF or K_I). It is known that SIF de-

scribes material resistance to brittle cracking. The stress intensity factor is investigated using specimens having a notch containing the fatigue crack at its tip and by applying the following stages of the experimental procedure: (a) precracking of fatigue zone, and (b) testing under monotonic tension [1]. Several types of specimen are used, i.e.: compact tension (CT) [2, 3]; disk-shaped [3]; single edge [3]; single or middle notched [2, 4]. In many experimental cases, the dimension of the specimen is limited by a material volume. Therefore, different sizes of specimen can be applied, i.e. standard [3], miniature (Fig. 1) [4, 5], or mini (Fig. 2) [6].

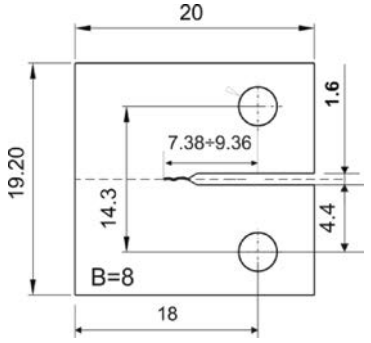

FIG. 1. Miniature compact specimen [5].

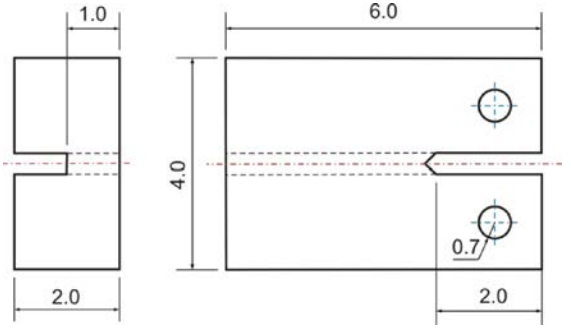

FIG. 2. Mini-compact specimen [6].

The objective of this paper is to determine a critical value of the stress intensity factor of a metal matrix composite (MMC) reinforced by the Saffil ceramic fibres.

As reported in [7, 8] the ultimate tensile strength and the Young's modulus of this type of reinforcement are equal to 1800 MPa and 300 GPa, respectively. The fibres can be applied in many engineering applications operated even at the temperature of up to 1 750°C [9]. The results of experiments also show that the content of the fibres influences material hardening. In the case of 2014 aluminium alloy, this effect, at both room and elevated temperature of 360°C,

was significantly higher than in the case of an unreinforced material [10]. Young's modulus achieved 22% increase at the fibre content equal to 10%, but for greater fibre volume fraction a gradual lowering of this parameter occurred. Finally, this parameter achieved 13% reduction compared to the base material without the reinforcement. Here, 10% of Al_2O_3 content caused 86% and 77% increase of the yield point and ultimate tensile strength determined at the temperature of 270°C, respectively.

2. Experimental results

The 44200 aluminium alloy [11] (AK11 according to Polish Standards PN-76/H-88027) reinforced by a different content of Al_2O_3 Saffil ceramic fibres, i.e. 10%, 15%, and 20%, were selected for investigation. All tests were performed using compact tension specimens (CT). With respect to a limited volume of the composite, the applied specimen was four times smaller than the typical one, and therefore, the experimental procedure contained two stages. The first step focused on examination of the specimen size by means of finite element analysis (FEA) and tests on the 40H steel, while the second stage concentrated on determining a critical value of the stress intensity factor of the composite.

2.1. Specimen and validation process

The compact tension specimen (Fig. 3), was designed on the basis of the ASTM [3] and PN-EN [12] guidelines. The specimen thickness was equal to the minimum recommended value, i.e. 6.5 mm, enabling examination of the material under plane strain state.

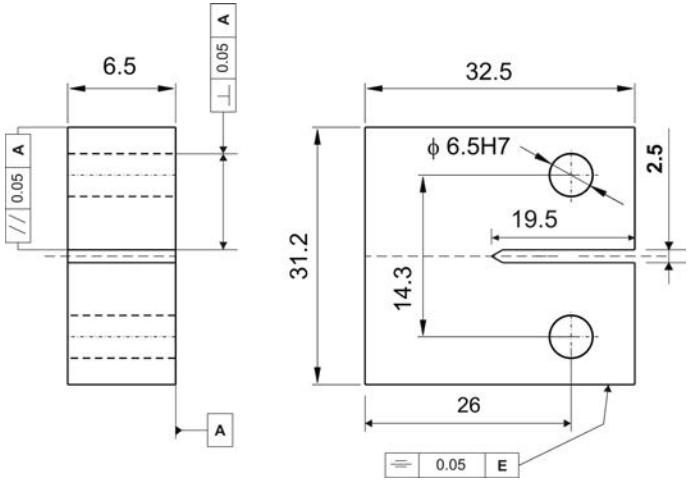

Fig. 3. Dimensions of the compact tension specimen (CT).

Further, the specimen geometry (Fig. 4a) was validated using FEA. The loading and boundary conditions were similar to those applied in the servo-hydraulic testing machine, as shown in Fig. 4b, c. The specimen was modelled as the fully elastic material and using 3D solid that was divided into 374088 3D elements stretched on 528467 nodes, Fig. 4c. Selected results, i.e. standardized values of the Huber-Mises-Hencky's effective stress at the tip of notch, are given in Fig. 5. The results indicate a typical distribution of the effective stress.

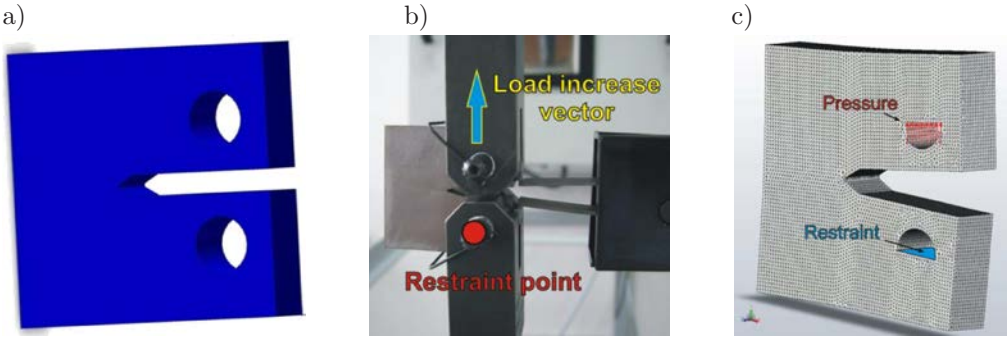

FIG. 4. Compact tension specimen: a) shape in 3D coordinates system, b) the real attachment, c) 3D mesh elements, simulated loading and boundary conditions by pressure and restraint.

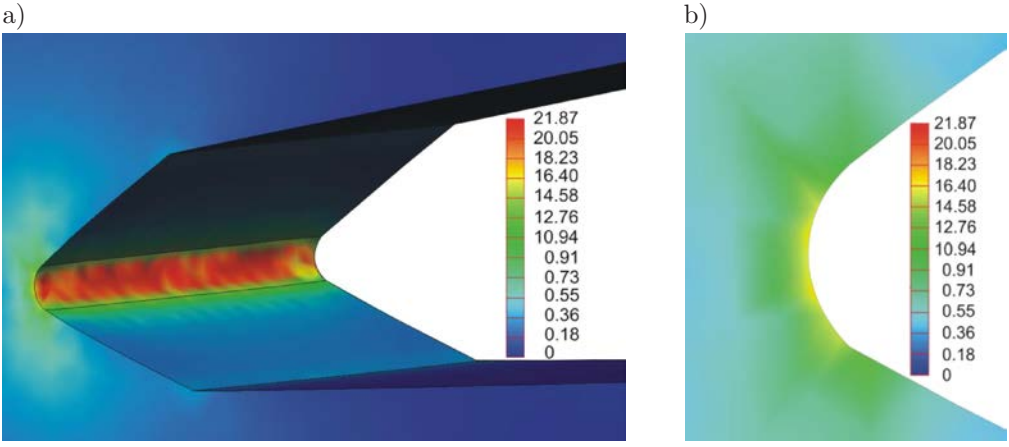

FIG. 5. Variation of the effective standardized stress at the tip of the notch, calculated using the Huber-Mises-Hencky's criterion, i.e.: a) 3D view, b) 2D view in front of the notch.

A validation of the specimen geometry on the basis of fracture toughness tests on the 40H steel was the first step of the procedure. For this type of material, a fatigue zone was successfully pre-cracked, Fig. 6a. Crack features of length equal

to 2.08 mm (Fig. 6b) and fatigue bands (Fig. 7) were determined at different magnification using the Scanning Electron Microscope (SEM). A critical value of the stress intensity factor of the 40H steel achieved the level of 38.8 MPa $m^{1/2}$ (close to the literature value equal to 40 MPa $m^{1/2}$).

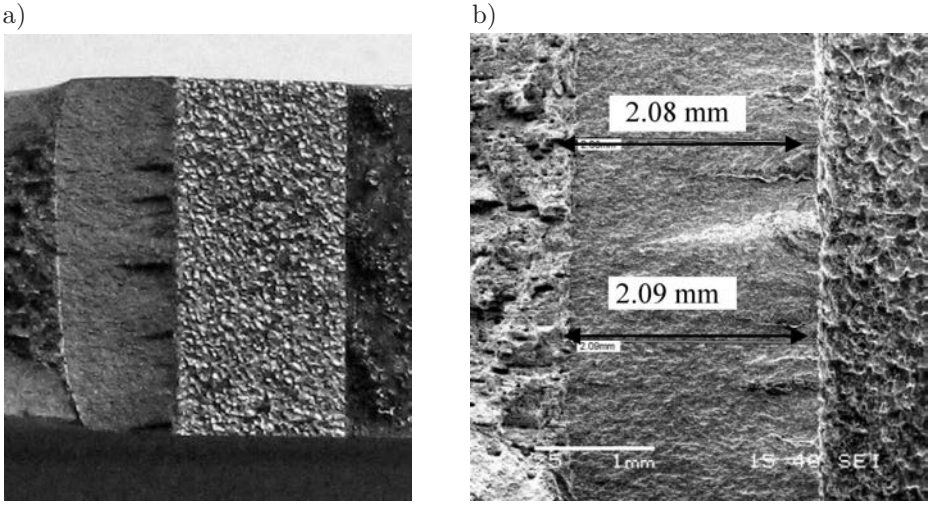

FIG. 6. Fracture surface of the 40H steel after fracture toughness testing: a) fatigue zone in macro scale, b) fatigue zone in micro scale (magnification 25×).

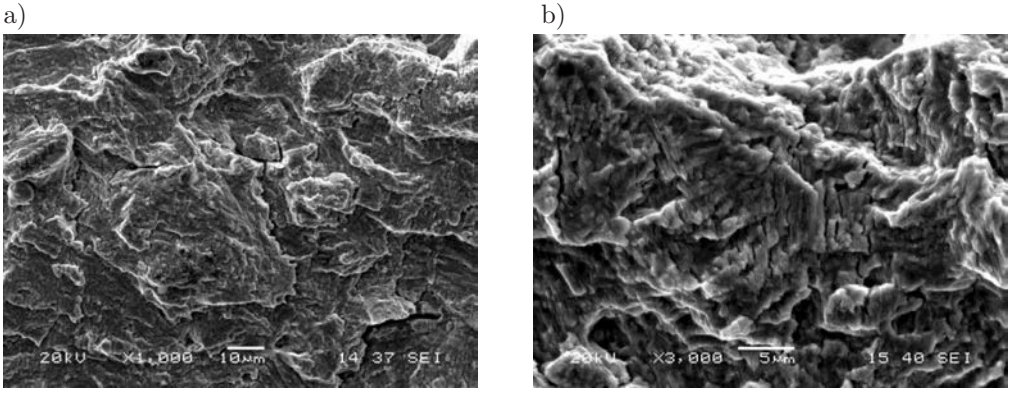

FIG. 7. Microscope image of a fatigue fracture surface of the 40H steel after fracture toughness testing: a) magnification 1000×, b) magnification 3000×.

2.2. Investigation of fracture toughness for the composites

In comparison to the typical engineering materials the composites were very difficult in machining. Therefore, preparation of the specimens (Figs. 3, 8a) at the recommended accuracy class required usage of more stages of the technological process than in the case of typical materials.

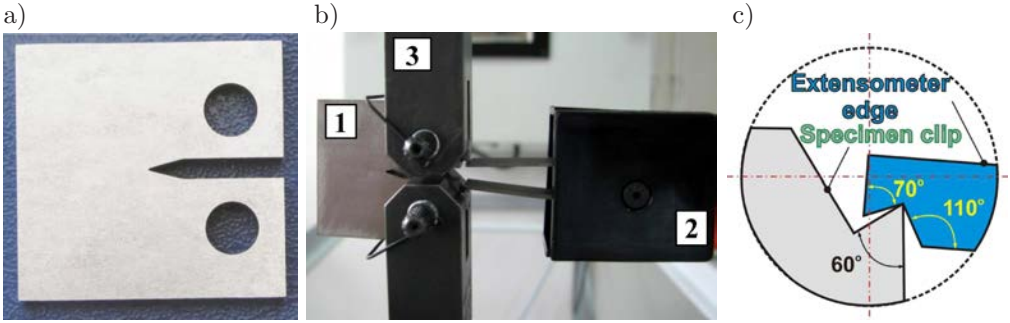

FIG. 8. Manufactured specimen: a) before testing, b) mounted in the loading system of the testing machine: 1 – specimen, 2 – extensometer, 3 – grips, c) knife-edge bearing (according to ASTM Standards [3]).

All fracture toughness tests were conducted using the 8802 Instron servo-hydraulic testing machine at room temperature. The specimens were mounted in the loading system by application of the special grips, Fig. 8b. Crack tip opening displacement was measured by means of the clip on knife edge extensometer of 10 mm gauge length; Figs. 8b, c.

In the case of all composite specimens the fatigue zone was successfully pre-cracked, and then, the materials were tested under monotonically increasing tensile force using the commercial programme for K_{IC} determination.

The crack propagated in the perpendicular direction to the opposite side of the specimen independently of the content of Al_2O_3 Saffil fibres (Figs. 9, 10, 12). Each specimen was observed at a different magnification to distinguish features of the fracture surface (Fig. 12b, 13). A macro-scale observation indicated several sections on this surface, i.e. (1) fatigue, (2) fracture, (3) sloping fracture, and (4) tearing; Figs. 12b, c. This expresses a disturbance of the plane strain state and exhibits composite fracture as that under mixed stress/strain conditions obtained.

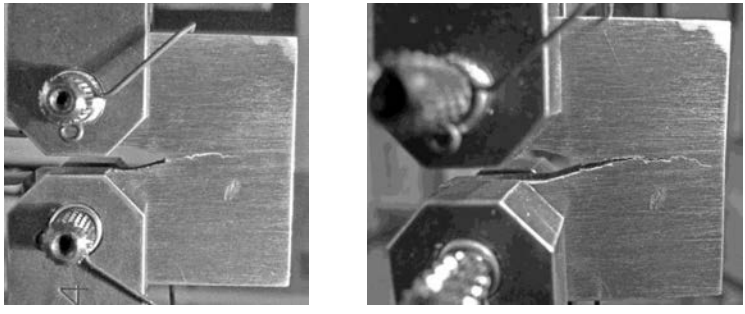

The first stage The last stage

FIG. 9. Rupture stages of the specimen made of the 44200+10% Al_2O_3 Saffil fibre composite.

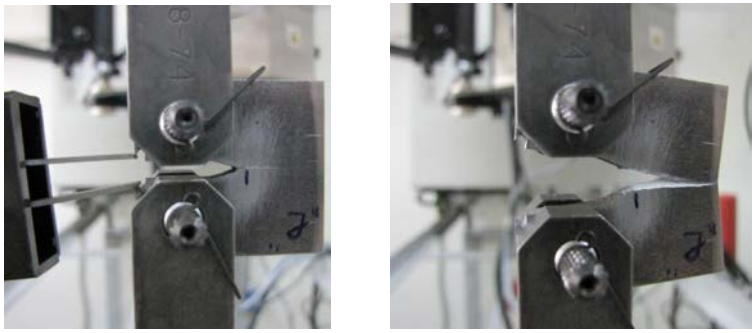

The first stage The last stage

FIG. 10. Rupture stages of the specimen made of the 44200+20% Al_2O_3 Saffil fibre composite.

a) b)

FIG. 11. Specimen made of the 44200+10% Saffil fibres composite after tests for K_{IC}: a) specimen, b) entire fracture surface.

a) b)

c)

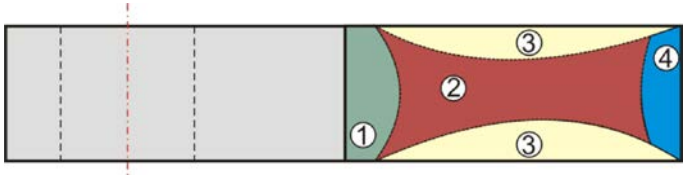

FIG. 12. Specimen made of the 44200+20% Saffil fibre composite after tests for K_{IC}: a) specimen, b) entire fracture surface, c) fracture surface scheme: 1 – fatigue area, 2 – fracture zone. 3 – sloping fracture surfaces, and 4 – tearing zone.

A microscopic analysis of the fatigue fracture surface was performed at magnification equal to 18 (Fig. 13a), 100 (Fig. 13b), 1000 (Fig. 14a), and 2500 (Fig. 14b). The results did not exhibit any of the typical features observed on the specimen surface after fatigue testing. Moreover, a local delamination of the structure was observed in the case of composite with 20% Al_2O_3 Saffil fibre content (Figs. 14a, b). It occurred in the form of voids between the matrix and fibres Fig. 14b.

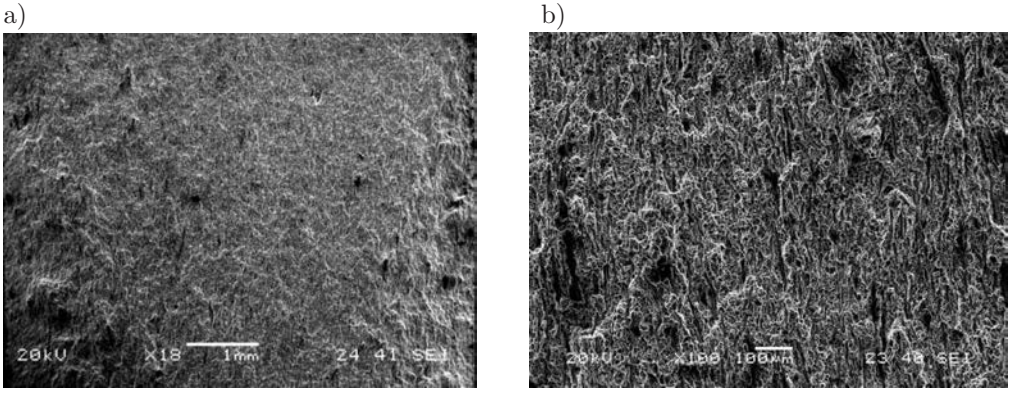

FIG. 13. Microscopic images of fatigue fracture surface of the 44200+20% Saffil fibre composite: a) magnification 18×, b) magnification 100×.

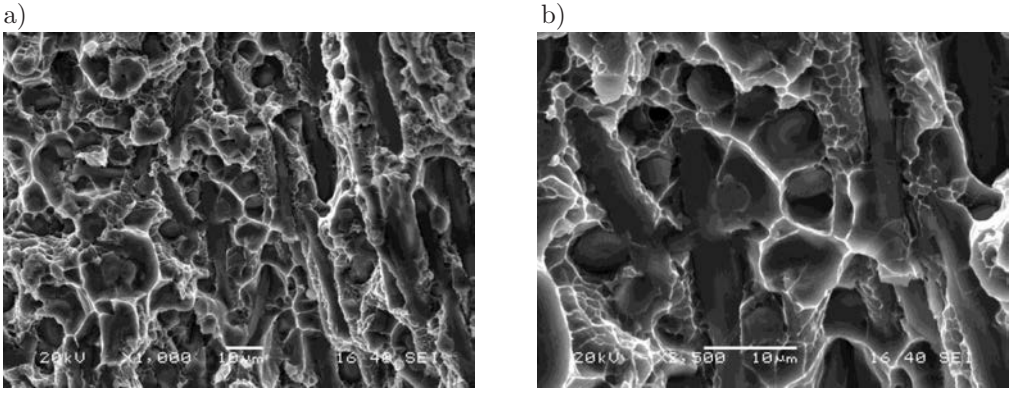

FIG. 14. Microscopic images of fatigue fracture surface of the 44200+20% Saffil fibre composite: a) magnification 1000×, b) magnification 2500×.

Variation of the tensile force versus crack tip opening displacement identifies the first mode of fracture, Fig. 15. An initial section of that characteristic was approximated using linear functions, Fig. 15b. This shows an influence of the Al_2O_3 Saffil fibres content on a variation of the proportionality coefficient. This parameter was increasing linearly with an increase of the fibres content. In the case of composite containing 10%, 15%, and 20% of the Al_2O_3 Saffil

fibres, it achieved the level of 10233.44, 10897.65, and 13120.61 respectively; Figs. 15b, 16.

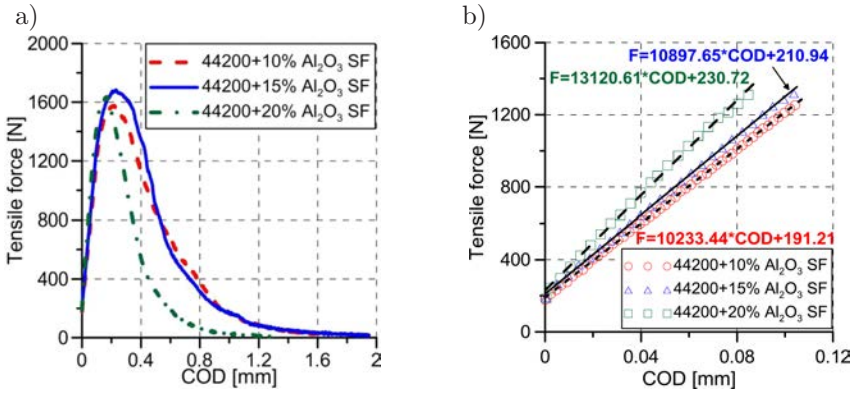

FIG. 15. Tensile force versus COD (a), linear section of diagrams presented in Fig. 15a.

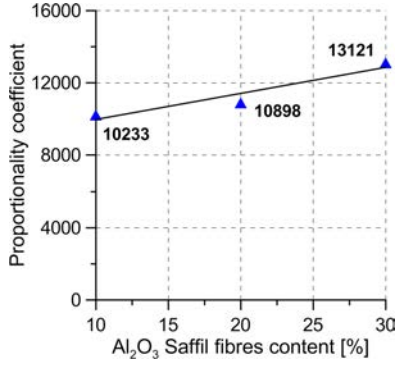

FIG. 16. Variations of the proportionality coefficient of function shown in Fig. 15b.

The relationship between the tensile force and crack tip opening displacement was analysed with respect to variation of the fracture energy. It was calculated as the area below the curves presented in Fig. 15. As shown in Fig. 17, this

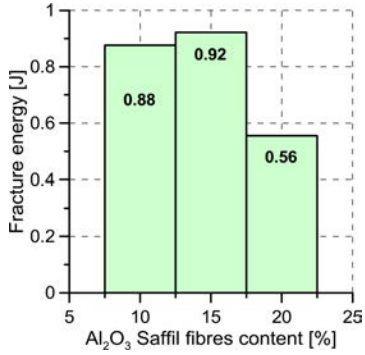

FIG. 17. Fracture energy against the Al_2O_3 Saffil fibres content.

parameter does not confirm any particular tendency, although variations of the proportionality coefficient were increasing linearly.

The critical values of the stress intensity factor of the 44200 aluminium alloy reinforced by various content of the Saffil fibres, i.e. 10% ,15%, 20%, reached the following levels: 12.201, 12.121, and 11.866 [MPam$^{1/2}$], respectively. It is easy to conclude, that these values are three times smaller than those determined for the 40H steel. It seems that the fracture toughness of the composites tested is not high enough to be use especially for the very responsible elements of engineering constructions.

3. Summary

The paper presents experimental data from the fracture toughness tests conducted on the 44200 casting aluminium alloy reinforced by the Al_2O_3 Saffil ceramic fibre. Analyses of the results make it possible to formulate the following remarks:

a) four times smaller specimen than the typical one can successfully be applied to determine a critical value of the stress intensity factor;
b) pre-cracked zone in the composite did not has typical features usually observed on the specimen surface after fatigue;
c) influence of the Al_2O_3 Saffil fibres content within the range from 10% to 20%, on the critical stress intensity factor was negligible small;
d) critical value of the stress intensity factor of the composite was three times smaller than that for the 40H steel achieved.

Acknowledgment

This paper was supported by the KomCerMet project (contract No. POIG. 01.03.01-14-013/08-00 founded by the Polish Ministry of Science and Higher Education) in the framework of the Operational Programme Innovative Economy in the years 2007–2013.

References

1. Dobrzański L., Nowosielski R., *Testing of metals and alloys*, vol. I, "Investigations of mechanical and physical properties" [in Polish], Silesia University of Technology, Gliwice 1986.
2. Doga B., Ceyhan U., Nikbin K.M., Petrovski B., Dean D.W., *European code of practice of creep crack initiation and growth testing of industrial relevant specimens*, Journal of ASTM International, **3**, 2, 20, 2006.

3. Standard Test Method for Plane-Strain Fracture Toughness of Metallic Materials, Annual Book of ASTM Standards, *Metals Test Methods and Analytical Procedures, Metals-Mechanical Testing: Elevated and Low-Temperature Tests*, Metallography, **03.01**, 509–539, 1993.

4. Kalluri S., Telesman J., *Characterization of fatigue crack initiation and propagation in Ti-6A1-4V with electrical potential drop technique*, NASA Technical Memorandum 100877, July 1988.

5. Golerthan S., Herberg D., Baruj A., Eggeler G., *Compact tension testing of martensitic/pseudoplastic NiTi shape memory alloys*, Materials Science Engineering, **481–482**, 156–159, 2008.

6. Bajaj D., Sundaram N., Arola D., *Striations resulting from fatigue crack growth in dentin*, [in:] Fractography of Glasses and Ceramics V: Ceramic Transactions, James R. Varner, George D. Quinn, Marlene Wightman, **199**, 2007.

7. Dieringa H., Hort N., Kainer K.U., *Compression creep of short fibre reinforced magnesium alloy AE42*, Composites, **3**, 7, 275–278, 2003.

8. Naplocha K., Kaczmar J.W., *Tribological properties of Al 7075 alloy based composites strengthened with Al_2O_3 fibres*, Archives of Foundry Engineering, **11**, Special Issue 2, 30/2, 153–158, 2011.

9. http://www.saffil.com/index/fibre_home/property_information.aspx.

10. Samuel M., *Reinforcement of recycled aluminium-alloy scrap with Saffil ceramic fibres*, Journal of Materials Processing Technology, **142**, 295–306, 2003.

11. PN-EN 1676:2011, *Aluminium and aluminium alloys – Alloy ingots for remelting – Specifications*, 2011.

12. PN-EN ISO 12737: 2011, *Metals – Fracture toughness at biaxial strain state*, 2011.

Received March 6, 2013; revised version June 11, 2013.

39th Solid Mechanics Conference

September 1–5, 2014
Zakopane, Poland

The Solid Mechanics Conferences have been organized by the Institute of Fundamental Technological Research since 1953. The Conferences have maintained high scientific standard and served as a forum for the exchange of ideas and research information. Traditionally, invited lectures have been presented by outstanding researchers at these Conferences. The aim of the Conference is to bring together researchers from different countries and to create for them the possibility for the presentation and discussion of scientific results from a wide area of solid mechanics, including the topics:

- biomechanics,
- computational aspects of mechanics,
- continuum mechanics, elasticity and plasticity,
- coupled problems and field theories of solids,
- dynamics of solids and structures,
- experimental mechanics,
- fracture, damage and fatigue,
- geomechanics,
- interfaces, thin layers and contact mechanics,
- mechanics of composites, porous media,
- micromechanics & thermodynamics of materials,
- nonlinear and stochastic dynamics,
- optimization, sensivity and reliability analysis,
- phase transitions and microstructures,
- smart materials and structures,
- structural mechanics.

Oral and poster sessions are planned.
The official language of the Conference is English.

Invited Plenary Lectures:

Holm Altenbach, Germany
Mechanics of Nanostructures

Josef Eberhardsteiner, Austria
Mechanical Behavior of Wood – a Bridge from Microstructure to Structural Applications by Means of Computational Methods

Narinder Gupta, India
Some Aspects of Large Deformations of Structures under Dynamic Loading

David Hayhurst, UK
High-temperature Continuum Damage Mechanics. Simulation of Materials and Components from Processing and Manufacture to Component Performance

Shaker Meguid, Canada
Multiscale Modelling of Multifunctional Nanocomposites for Aerospace Applications

Ryszard Pęcherski, Poland
Plastic Flow and Failure of Solids. Modelling Across Scales

Krzysztof Wiśniewski, Poland
Recent Improvements in Mixed/Enhanced Shell Elements with Drilling Rotation

Ramon Zaera Polo, Spain
Deformation of Dynamically Phase Transforming Metals in Adiabatic Conditions: Thermal Effects and Instabilities

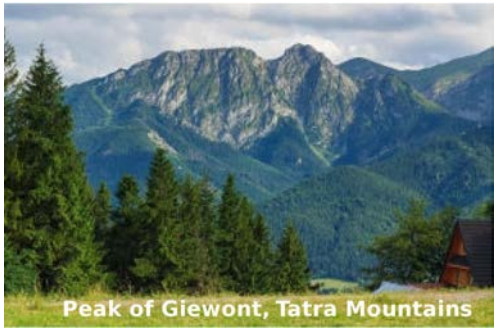

Scientific Committee:

• Janusz Badur	Institute of Fluid-Flow Machinery, Gdańsk
• Michał Basista	Institute of Fundamental Technological Research, Warsaw
• Adam Borkowski	Institute of Fundamental Technological Research, Warsaw
• Tadeusz Burczyński	Silesian University of Technology, Gliwice
• Paweł Dłużewski	Institute of Fundamental Technological Research, Warsaw
• Witold Gutkowski	Institute of Fundamental Technological Research, Warsaw
• Jan Holnicki-Szulc	Institute of Fundamental Technological Research, Warsaw
• Michał Kleiber	President of the Polish Academy of Sciences, Warsaw
• Witold Kosiński	Polish-Japanese Institute of Information Technology, Warsaw
• Zbigniew Kotulski	Warsaw University of Technology, Warsaw
• Piotr Kowalczyk	Institute of Fundamental Technological Research, Warsaw
• Zbigniew Kowalewski	Institute of Fundamental Technological Research, Warsaw
• Józef Kubik	Kazimierz Wielki University, Bydgoszcz
• Tomasz Łodygowski	Poznań University of Technology, Poznań
• Zenon Mróz	Institute of Fundamental Technological Research, Warsaw
• Andrzej Nowicki	Institute of Fundamental Technological Research, Warsaw
• Piotr Perzyna	Institute of Fundamental Technological Research, Warsaw
• Henryk Petryk	Institute of Fundamental Technological Research, Warsaw
• Ryszard Pęcherski	Institute of Fundamental Technological Research, Warsaw
• Elżbieta Pieczyska	Institute of Fundamental Technological Research, Warsaw
• Wojciech Pietraszkiewicz	Institute of Fluid-Flow Machinery, Gdańsk
• Maciej Pietrzyk	AGH University of Science and Technology, Cracow
• Jerzy Rojek	Institute of Fundamental Technological Research, Warsaw
• Błażej Skoczeń	Cracow University of Technology, Cracow
• Stanisław Stupkiewicz	Institute of Fundamental Technological Research, Warsaw
• Gwidon Szefer	Cracow University of Technology, Cracow
• Jacek Tejchman	Gdańsk University of Technology, Gdańsk
• Andrzej Tylikowski	Warsaw University of Technology, Warsaw
• Krzysztof Wiśniewski	Institute of Fundamental Technological Research, Warsaw

Organizing Committee: Zbigniew Kowalewski – Chairman
Zbigniew Ranachowski – Scientific Secretary

Managing assistants:
Urszula Czubacka
Paweł Grzywna
Dominik Kukla
Tomasz Libura
Agnieszka Rutecka
Jacek Widłaszewski
Joanna Żychowicz-Pokulniewicz

Abstracts

Abstracts should be submitted electronically on-line via

http://solmech2014.ippt.pan.pl/

Two-page camera-ready extended abstracts in English in accordance with the Word template are due by **February 28, 2014**. We encourage all authors to submit full length papers after the Conference for publication in *Archives of Mechanics* or *Engineering Transactions*. The papers will be subjected to the usual peer-review procedure.

Registration

Registration for the Conference should be performed on-line using the registration form available at

http://solmech2014.ippt.pan.pl/

Conference Fee

Registration fee:	before 31.05.2014	after 31.05.2014
Full	1800 PLN	2050 PLN
Student	1200 PLN	1450 PLN
Accompanying person	800 PLN	800 PLN

Registration fee includes:

- welcome reception, gala dinner, lunches, coffee and beverages during two breaks each day,
- admission to all sessions, conference materials,
- tour around Zakopane.

Student fee is eligible for junior scientists who have submitted an abstract and the Young Researcher Application Form, which should be sent to the Chairman of the Conference before May 31, 2014. Instructions how to reach Zakopane will be available on the Conference website.

Accommodation

Accommodation is not included in the Conference fee. A variety of hotels of different standards and convenient locations in Zakopane can be advised by the Conference Partner – Global Wings. Special conference rates are offered for rooms at selected hotels. Detailed information about the hotels location, room standards and prices can be found on Global Wings website. Registered participants may reserve rooms at these hotels after login at

http://www.globalwings.pl.

Venue, social programme:

As a conference site Zakopane, the fabulous capital of the Polish Tatra Mountains, was chosen. The Conference will be held at the *Hotel Belvedere* (the best hotel in Zakopane), located in the proximity of the town centre with instant access to marked pedestrian routes of the Tatra National Park. A variety of hotels and inns of different standards and prices are located in the vicinity of the Conference Venue. Among the traditionally organized facilities, a Welcome Party, Gala Dinner and excursions are foreseen.

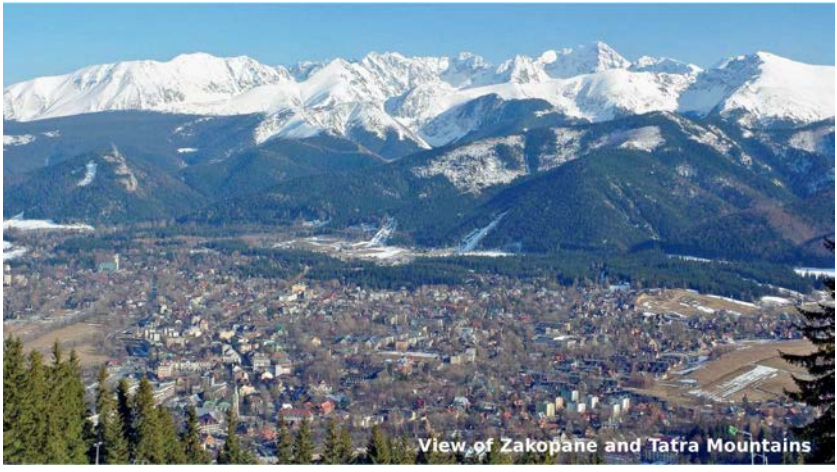

Conference Venue

Contact: Institute of Fundamental Technological Research
phone: +48 22 826 98 34 fax: +48 22 826 73 80
e-mail: solmech2014@ippt.pan.pl

Further informations & guidelines will be available at the Conference site:
www.solmech2014.ippt.pan.pl

DIRECTIONS FOR THE AUTHORS

The periodical *ENGINEERING TRANSACTIONS (ROZPRAWY INŻYNIERSKIE)* presents original papers which should not be published elsewhere.

As a rule, the volume of a paper should not exceed 40 000 typographic signs. The following directions are particularly important:

1. **The paper submitted for publication should be written in English.**
2. The title of the paper should be as short as possible. The text should be preceded by a brief introduction; it is also desirable that a list of notations used in the paper should be given.
3. Short papers should be divided into section and subsection, long papers into sections, subsections and points. Each section, subsection or point must bear a title.
4. The formula number consists of two figures: the first represents the section number and the other the formula number in that section. Thus the division into subsections does not influence the numbering of formulae. Only such formulae should be numbered to which the author refers throughout the paper. This also applies to the resulting formulae. The formula number should be written on the left-hand side of the formula; round brackets are necessary to avoid any misunderstanding. For instance, if the author refers to the third formula of the set (2.1), a subscript should be added to denote the formula, viz. $(2.1)_3$.
5. All the notations should be written very distinctly. Special care must be taken to distinguish between small and capital letters as precisely as possible. Semi-bold type must be underlined in black pencil. Explanations should be given on the margin of the manuscript in case of special type face.
6. Vectors are to be denoted by semi-bold type, transforms of the corresponding functions by tildes symbols. Trigonometric functions are denoted by sin, cos, tan and cot, inverse functions – by arc sin, arc cos, arc tan and arc cot; hyperbolic functions are denoted by sh, ch, th and cth, inverse functions – by Arsh, Arch, Arth and Arcth.
7. The figures in square brackets denote reference titles. Items appearing in the reference list should include the initials of the first name of the author and his surname, also the full of the paper (in the language of the original paper); moreover;
   a) In the case of books, the publisher's name, the place and year of publication should be given, e.g., 5. ZIEMBA S., *Vibration analysis*, PWN, Warszawa 1970;
   b) In the case of a periodical, the full title of the periodical, consecutive volume number, current issue number, pp. from ... to ..., year of publication should be mentioned; the annual volume number must be marked in semi-bold type as to distinguish it from the current issue number, e.g., 6. SOKOŁOWSKI M., *A thermoelastic problem for a strip with discontinuous boundary conditions*, Arch. Mech., **13**, 3, 337–354, 1961.
8. The authors should enclose a summary of the paper. The volume of the summary is to be about 100 words, also key words are requested.
9. The preferable format for the source file is TeX or LaTeX while MS Word is also acceptable. Separate files for the figures should be provided in one of the following formats: EPS or PostScript (preferable), PDF, TIFF, JPEG, BMP, of at least 300 DPI resolution. The figures should be in principle in gray-scale and only if necessary the color will be accepted.

Upon receipt of the paper, the Editorial Office forwards it to the reviewer. His opinion is the basis for the Editorial Committee to determine whether the paper can be accepted for publication or not.

Once the paper is printed, the issue of Engineering Transactions free of charge is sent to the author. Also the PDF file of the paper is forwarded by the e-mail to the authors.

Editorial Committee
ENGINEERING TRANSACTIONS